Dopaminergic modulation of superficial layer projection neuron excitability in the lateral entorhinal cortex

Laura Anne Harvey

Master of Philosophy

Keele University

December 2020

Contents Page

ABSTRACT

Projection neurons located in the superficial layers of the entorhinal cortex provide the hippocampus with nearly all its sensory input. This innervation occurs via multiple discrete pathways to different targets within the hippocampus, including the perforant and temporoammonic paths, as well as via direct projections to area CA2. This segregation of sensory information suggests that these input streams each play a separate role in declarative memory. The actions of modulatory neurotransmitters on the excitability of projection neurons in the entorhinal cortex may be instrumental in filtering the content of sensory signals destined for processing by different hippocampal subfields and, the lateral division of the entorhinal cortex receives dense dopaminergic innervation from the ventral tegmental area. But little is known about potential dopamine-mediated effects on the propagation of sensory information from the entorhinal cortex to the hippocampus. To determine this, multiple intracellular recording methods were used to assess the intrinsic excitability of principal neurons located in superficial layers II and III of the lateral entorhinal cortex in juvenile rat brain slices maintained in vitro before, during and after treatment with dopamine. Initial immunolabelling experiments using antibodies against the enzyme tyrosine hydroxylase confirmed the presence of catecholaminergic fibres in the superficial layers of the lateral entorhinal cortex, and that these fibres overlapped considerably with both the somata and neuropil of principal neurons in layers II and III. Moreover, there was a significant difference in the expression pattern of tyrosine hydroxylase-positive fibres across each cortical layer with fluorescent labelling highest in layers I, V and VI, followed next by layer III and then by layer II. This differential innervation pattern supports the notion that dopamine may modulate network activity within each layer of the lateral entorhinal cortex in a slightly different way. Although initial whole-cell recording experiments were somewhat inconclusive, there was a reliable suppression of spiking activity in superficial layer neurons following the addition of 100 µM dopamine to the bathing medium. More focal application of dopamine delivered via pressure injection directly to layer II and layer III neurons individually, however, suggested that neurons in layer III were more sensitive to the suppressive effects of dopamine on excitability. Most layer III neurons stopped spiking in response to ‘puffs’ of dopamine whereas layer II neurons were only mildly affected by the same treatment. The perforated patch clamp method was then used to assess the effects of dopamine on neuronal excitability in layer II and layer III projection neurons separately over an extended period (60 min). Bath-application of 100 µM dopamine for 10-min affected layer II and III neurons differently, with layer II neurons responding more strongly to treatment. In both layers, dopamine caused a significant attenuation of spiking activity, but only layer II neurons showed coincident changes in membrane potential and membrane resistance linked to the suppression of cell firing. Taken together, these findings show that the strength of dopaminergic projections to each layer of the lateral entorhinal cortex differs, and that this distinct pattern of innervation affects the excitability of layer II and layer III projection neurons in unique ways. As such, dopaminergic inputs to the lateral entorhinal cortex may serve to regulate the flow of sensory signals to different targets in the hippocampus depending on the salience of ongoing motivational, appetitive or affective factors known to recruit the mesocortical dopamine system.

Acknowledgements

I would like to express my deep gratitude to Dr Douglas Caruana and Dr John Butcher, my research supervisors throughout most of this work, for their scientific guidance, encouragement and useful critiques of this research.

I also wish to thank George Pettitt for his assistance in lab preparing stock solutions and Dafna Ljubotina for her work on tyrosine hydroxylase immunolabelling of dopamine fibres in the lateral entorhinal cortex.

Finally, I wish to extend thanks to family and friends around me who kept me focussed and motivated.

INTRODUCTION

Anatomy of the Entorhinal Cortex

The entorhinal cortex occupies a key position in the mammalian brain as the primary link between major sensory systems and the hippocampal formation (for review see Burwell, 2006; Canto, Wouterlood and Witter, 2008). It is believed that multiple sensory inputs are integrated into a single episode within entorhinal cortex circuits before being relayed to the hippocampal formation for integration with associated contextual, spatial and temporal cues (Canto and Witter, 2012; for review see Witter *et al.*, 2017). Based on this close synergy with the hippocampus (see **Figure 1** below), it is believed that the entorhinal cortex plays a pivotal role in the formation of new episodic memories (for review see Hasselmo, 2006; Canto, Wouterlood and Witter, 2008; Nilssen *et al*., 2019).

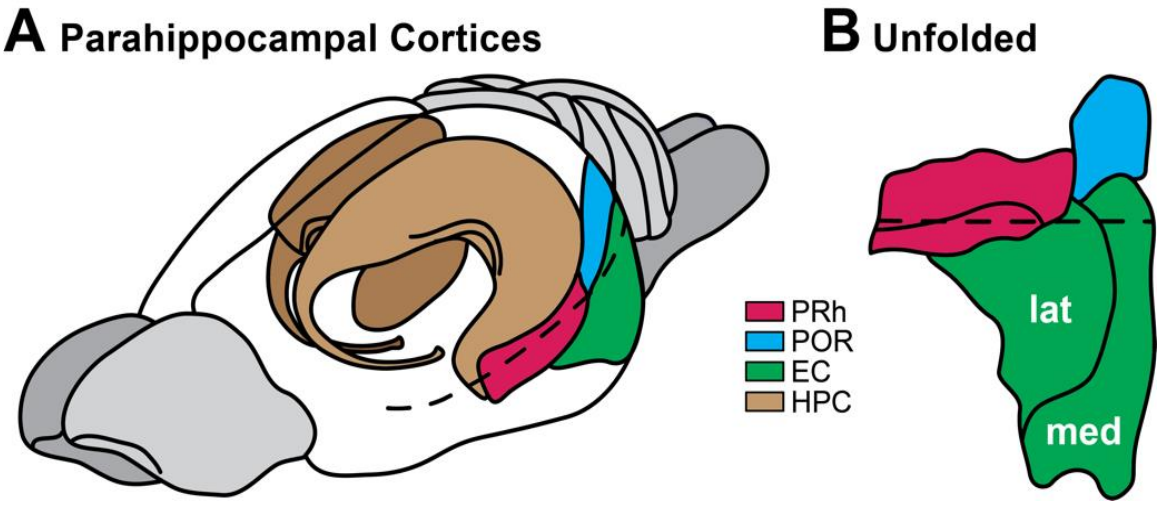

Figure 1. The parahippocampal cortices, including the entorhinal cortex, share rich interconnections with the hippocampus and play a key role in the formation of new declarative memories. *Diagram in* ***A*** *highlights the proximity of the parahippocampal cortices relative to the hippocampus (PRh, perirhinal cortex; POR, postrhinal cortex; EC, entorhinal cortex; and HPC, hippocampus). An unfolded view of the parahippocampal cortices highlighting both the medial (med) and lateral (lat) divisions of the entorhinal cortex, is shown in* ***B****.*

Like other cortical regions, the entorhinal cortex consists of six distinct layers, but there are several prominent anatomical and network features that set the entorhinal cortex apart from the rest of the neocortex. Firstly, the deep layers in most cortical regions tend to be output layers, but in the entorhinal cortex, this trend is reversed and it is neurons in the superficial layers (layers II and III, specifically) where the major projection neurons reside (Lingenhöhl and Finch, 1991; Solodkin and Van Hoesen, 1996). Secondly, neurons in more rostral locations appear clumped together into small clusters as opposed to being distributed more evenly (Blackstad, 1958; Steward, 1976; Wyss, 1981; Carboni and Lavelle, 2000). Layer IV of the entorhinal cortex also contains a layer that is completely devoid of cells known as the lamina dissecans, and this region is believed to be an artefact of a molecular layer that may have existed in the entorhinal cortex early on in mammalian evolution (Solodkin and Van Hoesen, 1996).

Brodmann was the first to propose that the entorhinal cortex consists of both a medial and a lateral division (for review see Canto, Wouterlood and Witter, 2008), with its name based on its

location relative to the rhinal sulcus. The word *'ento'* is derived from Latin roots meaning *'within'*. As such, the word *'entorhinal'* means literally, *'within the rhinal sulcus'*. Not only is the entorhinal cortex strongly interconnected with the hippocampus (see **Figure 2**), spatial and non-spatial information are processed separately by the medial and lateral divisions, respectively. For example, specialised cells, known as 'grid cells', have been discovered in the medial division, named aptly for their role in creating an internalised 'grid-like' map of external space (Hargreaves *et al.*, 2005; Iwase, Kitanishi and Mizuseki, 2020; for review see Moser, Kropff and Moser, 2008; Moser *et al.*, 2014; Fukawa *et al.*, 2020).

A defining feature of the entorhinal cortex is its rich interconnectivity with the hippocampus. Sensory inputs funnel into the superficial layers of both the medial and lateral divisions of the entorhinal cortex where it is believed the signals are integrated and processed independently before being transferred to the hippocampus. This propagation occurs via *multiple parallel streams*, including the perforant and temporoammonic paths (see **Figure 2** below). Interestingly, information that has been processed by the hippocampus is returned once more to the entorhinal cortex, to the deep layers (lavers V and VI), where it is more often than not relayed back to the same cortical and subcortical regions that provided the sensory information initially (for review see Canto, Wouterlood and Witter, 2008; Witter *et al.*, 2017; Nilssen *et al.*, 2019). There are also interlaminar connections that allow crosstalk between the deep and superficial layers, and this provides a powerful feedback mechanism for hippocampal output to regulate hippocampal input by modulating the responsivity of the superficial layers of the entorhinal cortex to new information entering the system (Kloosterman, van Haeften and Lopes da Silva, 2004). The entorhinal cortex functions as a gateway controlling the flow of information into and out of the hippocampus (for review see Burwell, 2006).

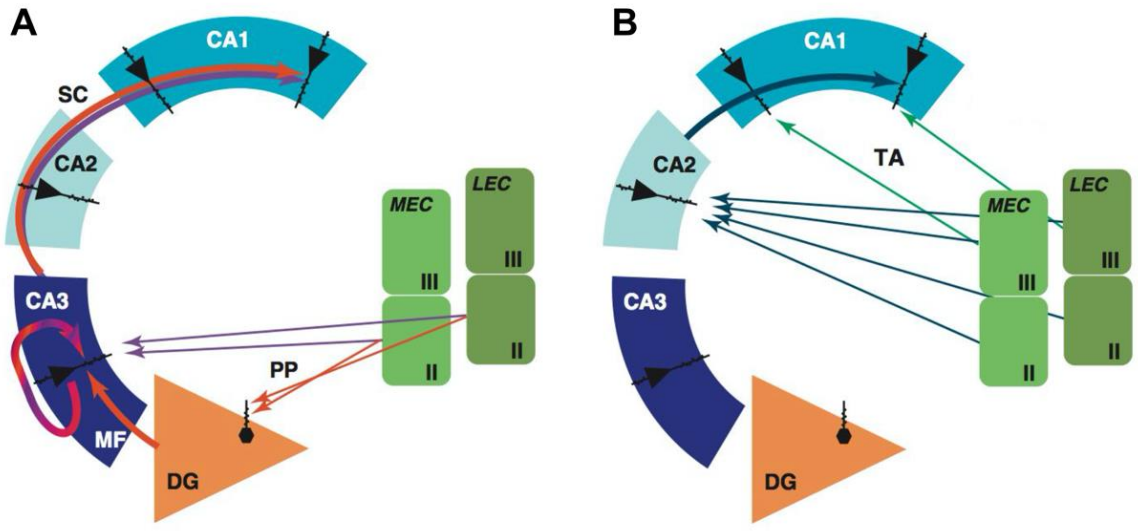

Figure 2. Superficial layer projection neurons in the medial and lateral entorhinal cortices provide the hippocampus with most of its sensory input. *The superficial layers of the entorhinal cortex act as a funnel to integrate multimodal sensory information and then project it to the hippocampus via the perforant (**A**; PP) or temporoammonic (**B**; TA) paths. More specifically, perforant path axons target either the dentate gyrus (DG) or area CA3 (**A**), temporoammonic inputs target neurons in area CA1 (**B**), and there is an additional cortical input from layers II and III of both the medial and lateral entorhinal cortices (MEC and LEC, respectively) that target area CA2 directly (**B**). In total, there are four discrete inputs to different hippocampal subfields, and it is believed that information carried by these independent streams may play*

differential roles in cognitive and mnemonic processing. Note: MF = mossy fibres and SC = Schaffer collaterals. Figure adapted from the review by Jones and McHugh, (2011).

Morphological and Electrophysiological Properties of Principal Neurons in the Lateral Entorhinal Cortex

Superficial layer projection neurons in both the medial and lateral entorhinal cortices play a critical role in information processing as they provide the hippocampus with much of its cortical sensory innervation. And as noted above, it is the axons that originate from these neurons that form both the perforant and temporoammonic paths to the hippocampus. Indeed, the compartmentalisation of information carried by these independent input streams to *different targets* in the hippocampus (see **Figure 2**) strongly suggests that these pathways each play a different role in cognitive and mnemonic processing. Although much is known about medial entorhinal cortex projection neurons and their role in both spatial processing and integration with hippocampal place cell networks, very little is known about lateral entorhinal cortical projection neurons and their unique contributions to declarative memory (but see Vandrey *et al*., 2020). A diverse array of neuronal phenotypes is found within superficial layers II and III of the lateral entorhinal cortex (see **Figure 3**), and experimental work by Tahvildari and Alonso (2005), as well as Canto and Witter (2012), highlights some of the diverse morphological and electrophysiological characteristics of principal neurons in layers II and III of the lateral division.

The superficial layers of the lateral entorhinal cortex contain a heterogeneous population of neurons that can project distally to the hippocampal formation, as well as collateralise extensively within the structure (see **Figure 3** below). The most notable difference between neurons found in layer II and those found in layer III relates to the branch patterns of their apical and basal dendritic trees. Neurons in layer III can branch extensively and ramify across multiple layers right through to layer V, whereas layer II neurons show more localised branching within the superficial layers (see **Figure 3**). This suggests that each layer may mediate separate functions related to sensory integration and mnemonic processing (Tahvildari and Alonso, 2005).

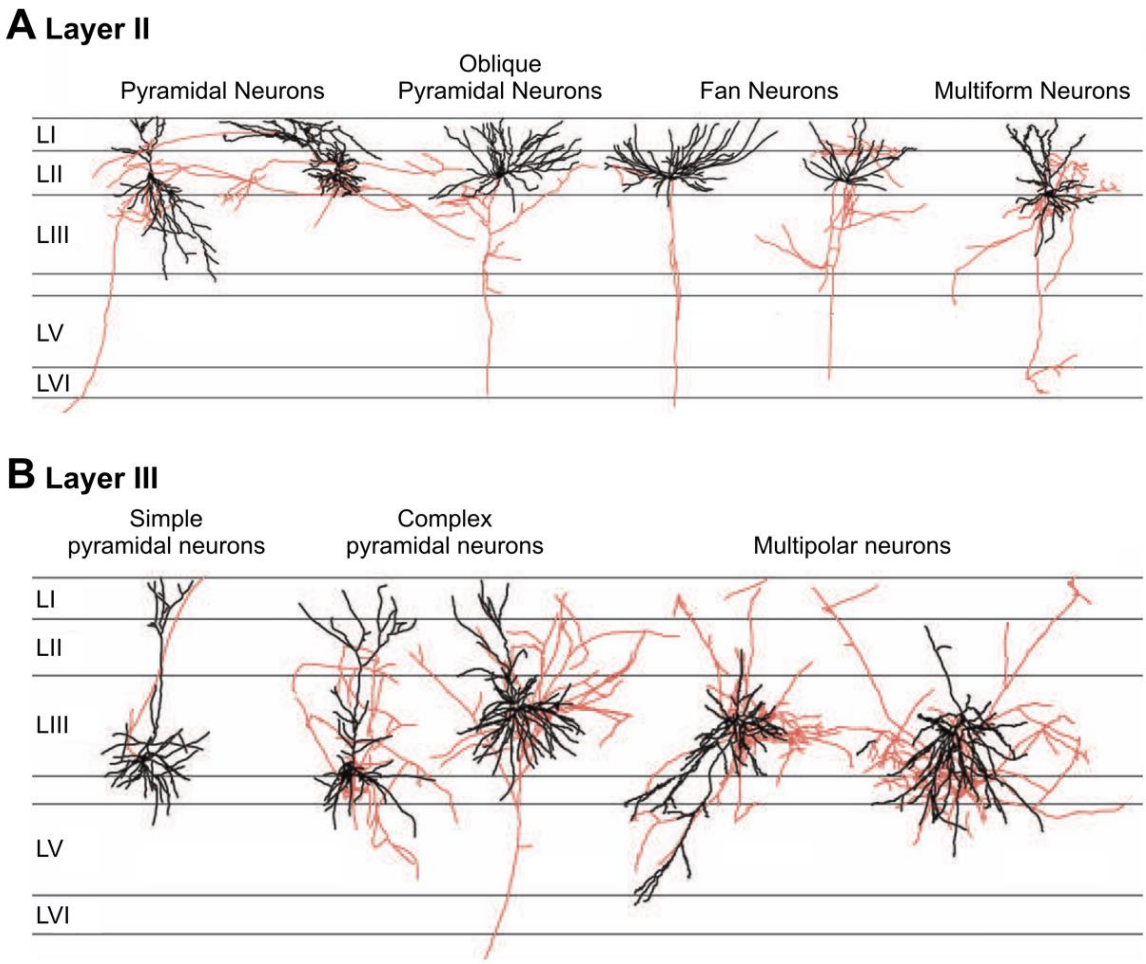

Figure 3. The superficial layers of the lateral entorhinal cortex contain a diverse array of neuronal phenotypes. *The projection neurons in layer II consist largely of pyramidal neurons, as well as the so-called 'fan' neurons (**A**). Layer III also contains a diverse mix of neuronal phenotypes, including various pyramidal neurons and multipolar neurons (**B**). Dendrites are coloured black whilst axons are in red. Data modified from Canto and Witter (2012).*

Both fan and pyramidal neurons are the principal cell types found in layer II (Tahvildari and Alonso, 2005; Canto and Witter, 2012). Multipolar cells also make up a large proportion of the superficial layers (most notably in layer III), but these neurons are much less consistent in terms of their morphological characteristics.

Layer II Fan Neurons

Morphologically, fan neurons have a polygon-shaped cell body with multiple thick dendrites extending vertically towards layer I, as well as horizontally to form a semi-circular shape (see **Figure 3A**, Fan Neurons). The dendrites of these neurons are also extremely spine dense. Although sharing a similar physical structure to medial entorhinal cortex layer II stellate cells, fan neurons lack the distinctive descending dendrites that give stellate cells their characteristic star-like appearance (Tahvildari and Alonso, 2005; Canto and Witter, 2012).

The electrophysiological characteristics of fan neurons in layer II of the lateral entorhinal cortex differ considerably from those of stellate cells found in the medial entorhinal cortex. As such, it is possible to classify these projection neurons based solely on their overall electrophysiological signatures. For example, layer II fan neurons have the most positive resting membrane potential

and the highest input resistance out of all the principal neurons in both layers II and III of the lateral entorhinal cortex (**Table 1**; Tahvildari and Alonso, 2005). They also exhibit much faster action potentials than pyramidal neurons, though the amplitude of the spikes tend to be much lower. In addition, fan neurons display modest time-dependent inward rectification in response to injection of hyperpolarising current. Indeed, a characteristic sag in the membrane potential from peak to steady-state values is observed typically in these neurons (**Table 1**; Tahvildari and Alonso, 2005). This is also coupled to instantaneous rectification observed during suprathreshold depolarisation. It should be noted that the inward rectification observed in fan neurons is significantly smaller than what is typically observed in stellate cells in the medial entorhinal cortex (Dickson *et al.*, 2000). Additionally, most fan cells elicit a single spike when first depolarised past threshold followed by phasic burst firing. The minority, however, spike like pyramidal neurons (see below) with an initial action potential doublet that precedes tonic burst firing (Tahvildari and Alonso, 2005).

Neuron Type	RMP (mV)	Input Resistance (MΩ)	Action Potential Threshold (mV)	Action Potential Amplitude (mV)	Sag (%)
LII Fan	–65.9 ± 0.58	57.3 ± 4.90	–45.4 ± 0.48	77.2 ± 0.86	11.5 ± 0.70
LII Pyramidal	–75.1 ± 0.42	41.6 ± 1.60	–44.6 ± 0.70	80.1 ± 2.10	0
Multiform	–70.0 ± 1.55	55.7 ± 6.85	–45.8 ± 0.50	78.0 ± 1.13	25 (in 1 cell)
LIII Pyramidal	–74.7 ± 0.39	50.0 ± 2.60	–45.9 ± 0.41	78.2 ± 1.04	0

Table 1. Summary of the main electrophysiological properties of superficial layer projection neurons in the lateral entorhinal cortex. *Values shown represent the mean ± SEM for fan neurons (n = 15), layer II pyramidal neurons (n = 9), multiform neurons (n = 7), and layer III pyramidal neurons (n = 25). RMP = Resting membrane potential; Sag is the measure of membrane rectification (%) in response to hyperpolarising current injection. Data modified from Tahvildari and Alonso, 2005.*

Layer II Pyramidal Neurons

Pyramidal neurons in layer II of the lateral entorhinal cortex are the second most abundant type of cell known to populate the superficial layers. They have a triangular or 'pyramid'-shaped cell body that is only slightly smaller than those of the fan neurons. They have a long apical dendrite that bifurcates within layer II whilst continuing to extend vertically to branch extensively in layer I and in the pia mater. They tend to have an equal spread of spiny dendrites both upwards and downwards replicating a typical rectangular-shaped dendritic tree. The basal dendrites, although thinner than the apical dendrite, branch horizontally within layer II and deeper into layer III (**Figure 3**; Tahvildari and Alonso, 2005). When depolarised, pyramidal neurons respond with an initial spike doublet followed by tonic burst firing. The pyramidal neurons in layer II have the most negative resting membrane potential and the lowest input resistance relative to other layer II neurons (see **Table 1**), and they display virtually no inward rectification in response to hyperpolarising current (Tahvildari and Alonso, 2005). This is in stark contrast to other pyramidal neurons found in area CA1 of the hippocampus (Chapman and Lacaille, 1999) or in the prefrontal cortex (Yang, Seamans and Gorelova, 1996).

Layer III Pyramidal Neurons

Pyramidal neurons are the predominant cell type found to reside in layer III of the lateral entorhinal cortex (Tahvildari and Alonso, 2005; Canto and Witter, 2012), and they are remarkably similar in terms of their overall morphology and electro-responsiveness to neurons found in layer III of the *medial* entorhinal cortex, as well as to pyramidal neurons in layer II of the lateral entorhinal cortex (see above; **Table 1**; Tahvildari and Alonso, 2005). In particular, pyramidal neurons in layer III of the lateral division have similar-sized somata as pyramidal neurons located more superficially in layer II, the primary apical dendrite of layer III pyramidal neurons is also thicker than its basal ones, with the apical dendrites branching extensively into layer II. The basal dendrites of layer III pyramidal neurons are much longer than those of layer II pyramidal neurons, but with fewer branches. These branches have been shown to spread into layer III and much deeper into layer V (Tahvildari and Alonso, 2005). The electrophysiological profiles of the various pyramidal neurons located in layer III are virtually identical to those outlined above for layer II pyramidal neurons (see **Table 1**; Tahvildari and Alonso, 2005).

Although many of the differences observed between the various types of projection neurons found in the superficial layers relate specifically to their overt morphological features, these differences may confer selective and important functional advantages. For instance, the diffuse arborisation of dendrites radiating from layer II fan neurons close to the pial surface suggests that these cells are targeted specifically by inputs terminating in layer I, whereas the branch patterns of layer II pyramidal neurons suggest they are targeted by afferents to both layer I *and* to layer II. Alternatively, neurons in layer III have longer and less collateralised dendrites suggesting they could be sites for interlaminar communication between layer II and layer III neurons directly, as well as with deeper layer neurons residing in layers V and VI. Indeed, such links between superficial and deep layer neurons are thought to support a powerful feedback mechanism through which hippocampal output to the deep layers of the entorhinal cortex can alter the responsivity of superficial layer neurons to new input (Kloosterman, van Haeften and Lopes da Silva, 2004; Tahvildari and Alonso, 2005; for review see Nilssen *et al.*, 2019).

From the discussion above, it is clear that the principal neurons residing in the medial and lateral divisions of the entorhinal cortex differ considerably from one another in terms of their overall morphology and electro-responsiveness, and that these differences confer important functional specialisations. Further, the segregation of sensory inputs to either the medial or lateral entorhinal cortices, together with the topographic specificity of outputs from these regions to different targets in the hippocampus, suggests that the medial and lateral divisions mediate qualitatively different types of information. Further, the lateral entorhinal cortex contributes mainly to odour and object identification whilst the medial entorhinal cortex plays a major role in spatial navigation. But a factor that is often overlooked, *yet absolutely central to these functions*, is the role of modulatory neurotransmitters in regulating key physiological mechanisms required for sensory and mnemonic processing (Deshmukh and Knierim, 2011). For example, cholinergic inputs from the medial septum that project to the hippocampus and entorhinal cortex are *essential* for optimal spatial memory processing by these structures (Egorov *et al.*, 2002; for review see Hasselmo *et al.*, 2002; Hasselmo, 2006). And yet, although it has been known since the late 1970s that dopaminergic neurons in the midbrain innervate the entorhinal cortex (Fallon, Koziell and Moore, 1978), little work has been done to explore the role of dopamine in modulating the excitability of superficial layer projection neurons in layers II and III of the lateral entorhinal cortex (but see Caruana and Chapman, 2008).

Dopaminergic Innervation of the Entorhinal Cortex

Neuromodulatory innervation provided by midbrain dopaminergic neurons is thought to play a

significant role in regulating neuronal activity related to reward-relevant stimuli, as well as to appetitive behaviour, mood and affect. In early anatomical studies, the exact boundaries of the ventral tegmental were difficult to demarcate with any precision due, in part, to the presence of multiple neurotransmitters, receptor subtypes and neuronal phenotypes present within its presumed borders. Initial reports suggested that the ventral tegmental area was composed of up to 29,000 individual neurons, bilaterally, and of these, 18,000 neurons located within the central third of the structure were shown to contain tyrosine hydroxylase (for review see Oades and Halliday, 1987). The medial division of the ventral tegmental area contains a cluster of dopaminergic neurons known, collectively, as the A10 cell group, and these neurons were shown to send dopaminergic projections to a number of cortical and subcortical targets (See **Figure 4** below), including the lateral entorhinal cortex. Additionally, it has been shown that there is significant homology across mammalian species (including, humans, primates and rodents) in terms of the organisation and topography of A10 efferents to widespread targets throughout the brain (for review see Oades and Halliday, 1987).

Axons from A10 dopaminergic neurons project towards the basal forebrain, but some of these projections bifurcate at the medial forebrain bundle to innervate the entorhinal cortex. This branch is considered part of the mesocortical system that includes dopaminergic efferents to the prefrontal cortex (Swanson, 1982; for review see Oades and Halliday, 1987). Early anatomical reports demonstrated that dopaminergic projections to the cortex terminated in the deep layers of the frontal cortices, as well as in the superficial layers of the lateral entorhinal cortex (Lindvall *et al.*, 1974). Dopaminergic terminals are evident in the anterior cingulate cortex and ventral entorhinal cortex (containing mostly lateral entorhinal cortex), as well as along the rhinal fissure (Lindvall *et al*., 1974). Those in the entorhinal region have similar morphology to dopamine projections in the frontal cortex, but they form clusters around cell islands observed mainly in layers II and III. Focal lesions to the A8, A9 and A10 cell groups as defined by Fuxe (1965) presents evidence for dopaminergic projections forming very directed and deliberate connections with specific brain regions (Swanson, 1982). For example, dopaminergic axons innervate the entorhinal cortex via a path running adjacent to, but in the reverse direction of, the amygdalofugal pathway (Lindvall *et al*., 1974).

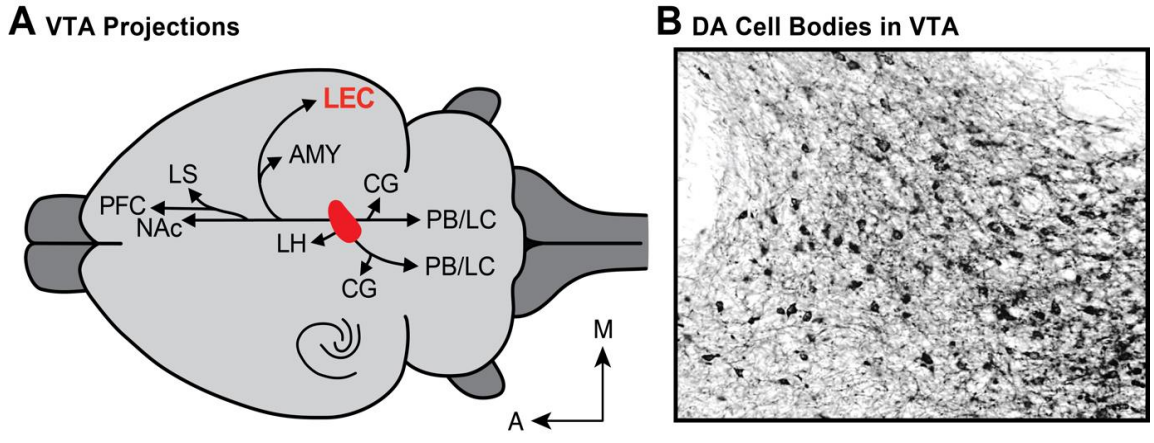

Figure 4. The ventral tegmental area innervates multiple cortical and subcortical structures, including the lateral entorhinal cortex. *Mesocortical dopaminergic projections from the A10 cell group in the ventral tegmental area (VTA, in red) innervate the lateral entorhinal cortex (LEC). The schematic diagram in* ***A*** *(adapted from Swanson (1982)) highlights both the cortical and subcortical targets of the VTA (VTA projections in black). The photomicrograph in* ***B*** *shows tyrosine-hydroxylase immunoreactivity labelling dopaminergic cell bodies in the VTA (D Caruana unpublished observation). Note: M = medial; A = anterior;*

Amygdala (AMY); central gray (CG); lateral habenula (LH); lateral septum (LS); nucleus accumbens (NAc); parabrachial nucleus/locus coeruleus (PB/LC); prefrontal cortex (PFC).

Dopamine receptors are found on many neuron types in the brain, including on principal neurons in the lateral entorhinal cortex. D_1-like receptors are found primarily on pyramidal cells in the prefrontal cortex with dopamine having a much higher binding affinity for D_5 receptors than D_1 receptors (for review see Seamans and Yang, 2004). All dopamine receptors are metabotropic, consisting of seven transmembrane regions. There are five main dopamine receptor subtypes: D_1 through to D_5. They are separated functionally and mechanistically based on their G-protein configuration. D_1-like receptors initiate signalling cascades that lead to a facilitation of synaptic transmission whereas D_2-like receptors lead to a suppression (Glovaci and Chapman, 2015, 2019; for review see Seamans and Yang, 2004). Both D_1 and D_5 receptors consist of a longer third cytoplasmic loop and carboxyl tail (see **Figure 5A** below) and therefore belong to the G_S- and G_{Olf}-coupled D_1 receptor (D_1R) family. D_2, D_3 and D_4 receptors belong to the $G_{i/o}$-coupled D_2 receptor (D_2R) family due to the presence of a much shorter cytoplasmic loop and carboxyl group. The divide of dopamine receptors seemingly favours D_1-like receptors as they are three times more prominent in the lateral entorhinal cortex than D_2-like receptors (Boyson, McGonigle and Molinoff, 1986; Richfield, Penney and Young, 1989). However, D_1Rs have a lower affinity for dopamine compared to D_2Rs. As a result, more dopamine is needed to activate D_1Rs if it is phasic release, tonic dopamine delivery is best suited for D_2R activation (for review see Subramaniyan and Dani, 2015).

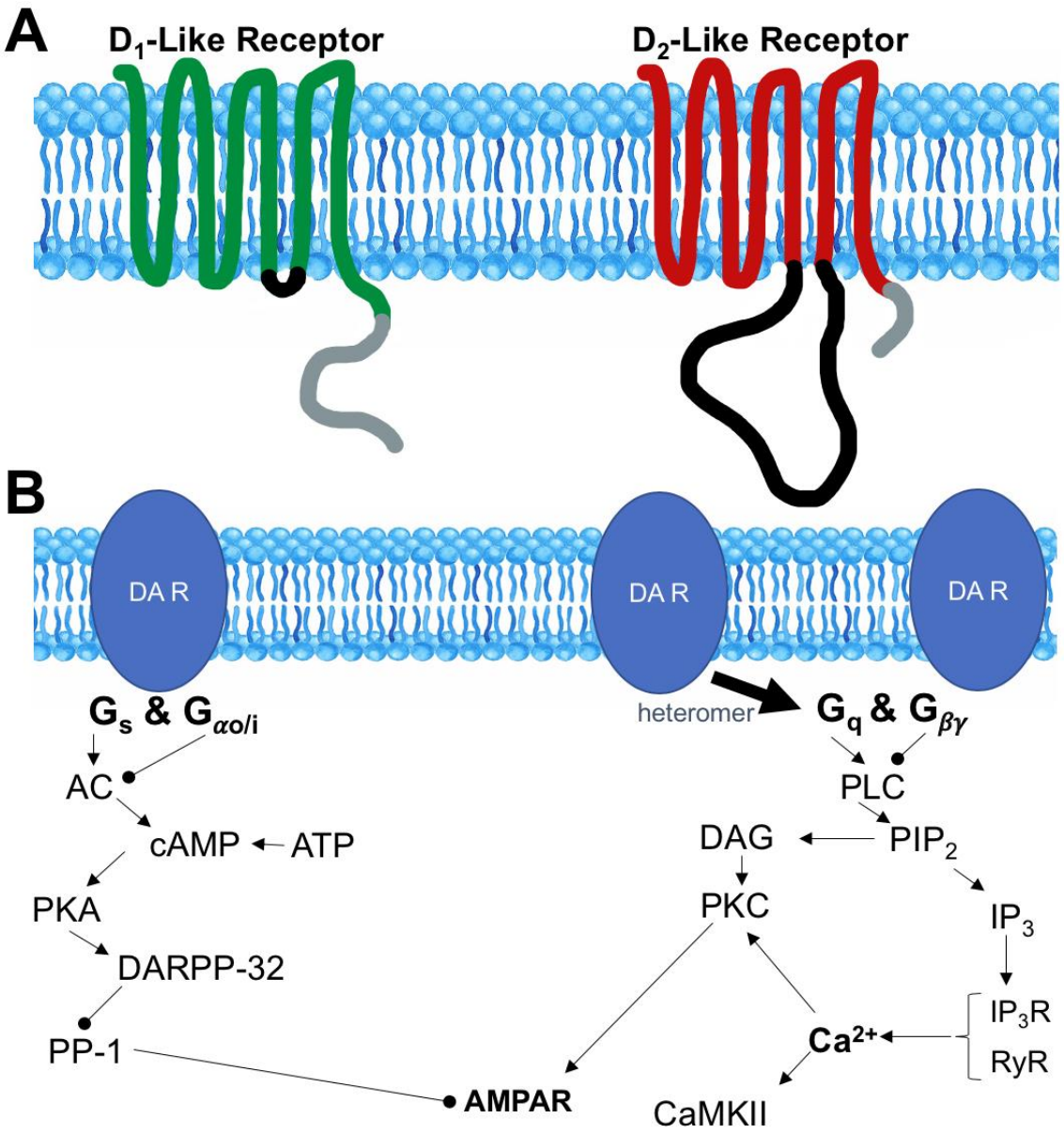

Figure 5. Schematic representation of dopamine receptor structure, including known intracellular signalling pathways*. D_1-like receptors have an elongated carboxyl tail (**A**, grey) compared to D_2-like receptors, however, the cytoplasmic loop is not as long (**A**, black). There are two independent pathways linked to activation of these two receptor families. Activation (arrowhead) of $G_{s,}$ via D_1-like receptors, leads to increased activity of adenyl cyclase (AC). However, stimulation of $G_{\alpha i/o}$ (dotted head) produces the opposite effect and inhibits activity of AC (**B**, left). If there is increased activation of AC this leads to an upregulation of protein kinase A (PKA), and subsequent activation of dopamine- and cAMP-regulated phosphoprotein 32 (DARPP-32). DARPP-32 downregulates protein phosphatase 1 (PP-1) activity to affect synaptic function by consequential disinhibition of α-amino-3-hydroxy-5-methyl-4-isoxazolepropionic acid (AMPA) receptors. In contrast, activation of D_2-like receptors signals, via phospholipase C (PLC), to regulate levels of protein kinase C (PKC) and inositol triphosphate (IP_3; **B**, right). PKC modulates AMPA receptor function directly, whereas IP_3 leads to an upregulation of intracellular calcium (Ca^{2+}) from internal stores. Enhanced intracellular Ca^{2+} can lead to activation of calcium calmodulin dependent protein kinase II (CaMKII), as well as PKC, both of which regulate AMPA receptor function to affect synaptic transmission. Note: Arrowheads are excitatory and dotted heads are inhibitory (Adapted from Hasbi, O'Dowd and George, 2010; Glovaci and Chapman, 2015; and reviews by Neve, Seamans and Trantham-Davidson, 2004; Beaulieu, Espinoza and Gainetdinov, 2015).*

Dopaminergic Modulation of Lateral Entorhinal Cortex Function

The potential for dopamine to act as a key mediator affecting the propagation of sensory signals to the hippocampus was first proposed over 30 years ago when neuroanatomists initially characterised dopaminergic inputs to the superficial layers of the entorhinal cortex (for review see Oades and Haliday, 1987). However, surprisingly little has been done in the intervening years to test this hypothesis directly. Early reports assessing the modulatory role of dopamine on entorhinal cortex function focussed specifically on the medial entorhinal cortex. In these studies, the effects of bath-applied dopamine were assessed on glutamate-mediated synaptic transmission in the superficial layers. Pralong and Jones (1993) showed that concentrations of 100 and 500 µM dopamine caused a potent suppression of synaptic responses in layer II fan neurons, and this suppression was mediated, in part, by a change in the membrane resistance of principal cells. Similar inhibitory effects of dopamine on excitatory synaptic transmission have also been observed in layer III, though it was concluded that the suppression was mediated by a dopamine-induced change in the release probability of glutamate, as there was a coincident increase in paired-pulse facilitation observed (Stenkamp, Heinemann and Schmitz, 1998). The results of these two studies were the first to suggest that dopamine may act as a gate to attenuate sensory integration in the entorhinal cortex by modulating synaptic efficacy in the superficial layers.

The powerful suppressive effects of dopamine on synaptic function were later confirmed in the lateral division of the entorhinal cortex. Bath-application of high concentrations of dopamine (50 to 100 µM) were sufficient to significantly reduce the amplitude of synaptic responses *in vitro* (Caruana *et al.*, 2006; Caruana and Chapman, 2008). Interestingly, the effects of dopamine were concentration-dependent *and bidirectional*. Low concentrations of dopamine (between 1 and 10 µM) enhanced synaptic transmission in layer II of the lateral entorhinal cortex (Caruana *et al*., 2006; Caruana and Chapman, 2008; Glovaci, Caruana and Chapman, 2014), and this was shown to be related to a D_1 receptor-mediated release of calcium from internal stores (Glovaci and Chapman, 2019). Additionally, enhancing extracellular levels of dopamine in the lateral entorhinal cortex *in vivo* were shown to block both activity-dependent long-term synaptic potentiation and long-term depression, though the precise mechanism underlying these effects remains unclear (Caruana *et al*., 2006; Caruana and Chapman, 2008).

Much less is known, though, about putative dopamine-mediated effects on the propagation of sensory information from the entorhinal cortex to the rest of the hippocampal formation. Previous work has shown that bath-applied dopamine (100 µM) reduces the number of action potentials elicited by layer II fan neurons in response to suprathreshold current injection, and that this effect is mediated by a dopamine-induced change in potassium currents regulating membrane resistance (Caruana and Chapman, 2008; but see also Batallán-Burrowes and Chapman, 2018). Similar suppressive effects on intrinsic excitability have also been observed in layer V neurons, but these effects were shown to depend on a dopamine-mediated facilitation of the hyperpolarization-activated cation current (I_h) (Rosenkranz and Johnston, 2006).

Current Study

As highlighted above, the data available exploring the modulatory effects of dopamine on synaptic transmission and intrinsic excitability of superficial layer projection neurons are extremely limited given the potential importance of dopamine to cognitive and mnemonic function in other regions of the brain, including the hippocampus and prefrontal cortex. Dopamine-mediated changes in sensory processing by entorhinal cortex circuits represents a novel mechanism for regulating the

propagation of processed signals to the hippocampus. And given the compartmentalisation of superficial layer efferents to different targets within the hippocampus, dopamine is certainly well-poised to act as a key mediator to direct sensory information flow during the encoding of new declarative memories. As such, the goal of this study was to further assess the effects of dopamine on the intrinsic excitability of superficial layer projection neurons in slices of the parahippocampal cortices containing the lateral entorhinal cortex, *in vitro*. A combination of intracellular recording techniques was used here to determine how dopamine affects the propagation of sensory information to the hippocampus, and whether dopamine influences the excitability of layer II versus layer III projection neurons differently.

MATERIALS AND METHODS

Ethics Statement

All procedures described below adhered strictly to the guidelines outlined in the UK Animal (Scientific Procedures) Act 1986, and every effort was made to minimise distress in experimental animals prior to euthanasia. Pre-weaned male and female Sprague Dawley rat pups were housed as single litters with their dam in the Central Animal Facility at Keele University. Animals were kept on a 12-hour light-dark cycle with lights on at 08:00, and dams had access to food and water *ad libitum* throughout testing.

A single rat brain was dissected and sliced early in the morning on each test day. The posteroventral portion of the temporal lobes, including the hippocampal formation and parahippocampal cortices, were used for experiments described below, and slices containing different brain regions were utilised by others in the lab (and department) for additional experimental work. The lateral division of the entorhinal cortex occupies a large proportion of the posteroventral temporal lobes (Paxinos and Watson, 2007) which allowed for numerous slices of tissue to be prepared from a single rat brain (between 6 and 8 slice pairs, bilaterally). As such, there was ample tissue available for experimental purposes, and little tissue was ever wasted.

Tissue Slices

The methods for harvesting and slicing rat brain tissue described below were similar to those used previously (Caruana and Chapman, 2008; Caruana, Warburton and Bashir, 2011; Caruana, D. A., Dudek, S. M., 2020). Both male and female Sprague Dawley rats aged between postnatal days 14 and 22 were used for this study. On a given test day, a single animal was brought to the lab and euthanised by Schedule 1. After decapitation, the brain was dissected rapidly and placed into a beaker containing oxygenated (95% O_2 and 5% CO_2) and ice cold (~4 °C) sucrose-substituted artificial cerebrospinal fluid (ACSF), comprised of (in mM): 2 KCl, 1.25 NaH_2PO_4, 1 $MgCl_2$, 1 $CaCl_2$, 26 $NaHCO_3$, 240 sucrose, and 10 D-glucose. All chemicals were obtained from Sigma-Aldrich unless noted otherwise. Next, the dissected brain was placed on ACSF-soaked filter paper positioned atop a glass petri dish packed with ice, and a single-edged razor blade was used to block it into smaller segments. First, two coronal cuts were made to remove the cerebellum and the most rostral portion of the frontal lobes. Following this was a single horizontal cut to remove enough of the dorsal cerebral cortex to allow the brain to sit flat when flipped upside down for mounting. Finally, a sagittal cut was made along the longitudinal fissure to separate the hemispheres. The two blocks of tissue containing both the left and right medial temporal lobes were then superglued to a mounting plate in front of a SYLGARD elastomer support block and secured to a vibrating blade microtome (VT1000S, Leica Systems) for slicing. Horizontal sections containing the hippocampal formation and parahippocampal cortices, including both the medial and lateral divisions of the entorhinal cortex, were cut to a thickness of 340 µm each. These slices were then transferred to a holding chamber and placed atop a nylon net submerged in oxygenated (95% O_2 and 5% CO_2) and warmed (30 to 32 °C) ACSF, containing (in mM): 124 NaCl, 2.5 KCl, 1.25 NaH_2PO_4, 2 $MgCl_2$, 2 $CaCl_2$, 26 $NaHCO_3$, and 17 D-glucose. Slices recovered for at least 60 minutes prior to use.

Following recovery, individual slices were placed in the recording chamber and visualised using an upright microscope (BX51WI, Olympus-Keymed) equipped with differential interference contrast optics, a 40x water-immersion objective and a near-infrared camera (IR-1000E, Dage-MTI). Once inside the chamber, slices were secured with a stainless-steel and Lycra slice anchor (SHD-42/15,

World Precision Instruments) and perfused continuously with oxygenated ACSF at a rate of 2 mL/min. Up to four separate reservoirs were available to deliver different solutions to the slice depending on experimental conditions. A 4-channel pinch-valve gravity perfusion system (Valve Commander VC3, ALA Scientific Instruments Inc.) was used to control solution changes manually during testing. Reservoirs were switched using a control pad, and flow rate was regulated manually by adjusting a pinch-clamp and thumb screw assembly rigged directly to the main perfusion line. ACSF was heated by an inline solution heater (SH-27B, Warner Instruments) just prior to entering the recording chamber, and the temperature of the bath was maintained at 30 to 32 °C by an automatic temperature controller (TC-324C, Warner Instruments) connected to a feedback thermistor positioned directly in the bath close to the slice.

Electrophysiology Experiments

I. Whole-Cell Patch Clamp Recordings

Methods for obtaining whole-cell patch-clamp recordings were similar to those described previously (Caruana and Dudek, 2020; Caruana, Warburton and Bashir, 2011; Caruana and Chapman, 2008). Recording electrodes were prepared from borosilicate glass (1.5 mm OD; 3-8 MΩ; Harvard Apparatus) using a horizontal micropipette puller (P-1000, Sutter Instruments, USA) and filled with a solution containing (in mM): 120 K-gluconate, 10 KCl, 3 $MgCl_2$, 0.5 EGTA, 40 HEPES, 2 Na^+-ATP, and 0.3 Na^+-GTP, as well as 5 mg/mL biocytin for subsequent streptavidin labelling work (described below; final osmolarity of 270-280 mOsm with pH adjusted to 7.2 using KOH). Slices were visualised on a monitor, and gross anatomical landmarks (such as the rhinal fissure) were compared under low magnification (4x) to corresponding reference plates found in the atlas of Paxinos and Watson (2007) so the precise location of the lateral entorhinal cortex could be identified. The recording electrode was then placed in close contact with the soma of individual neurons (visualised under 40x magnification) located in either layer II or layer III. Negative pressure was applied to the membrane using gentle suction under voltage clamp, which provided electrical control of the membrane potential and measure of the subsequent currents, to form a tight seal (≥ 1 GΩ). Whole-cell configuration was achieved by increased suction (see **Figure 6A** below).

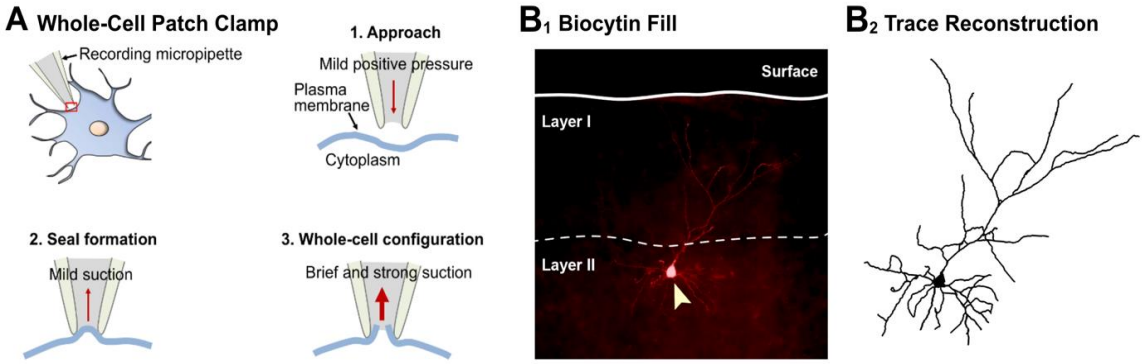

Figure 6. The whole-cell patch clamp method involves a slight disruption of the neuronal membrane to gain electrical access to the interior of the cell. *Under visual guidance, a recording micropipette is placed in close contact with the soma of a neuron. Mild positive pressure is applied to remove debris from the surface of the cell (**A**1. Approach). A switch to mild negative pressure facilitates formation of a tight seal (≥ 1 GΩ) between the tip of the micropipette and the neuronal membrane (**A**2. Seal formation). Strong negative pressure ruptures the membrane allowing the contents of the recording electrode (and AgCl recording lead) to come into contact with the intracellular medium (**A**3. Whole-cell configuration). Biocytin, included in the intracellular recording solution, diffuses into a patched neuron and can be processed for streptavidin*

*fluorescent labelling to visualise the morphological features of the cell (**B**$_1$). Shown in **B** is a small pyramidal neuron located in layer II of the lateral entorhinal cortex labelled using a streptavidin conjugate. Images of labelled neurons can be loaded into Fiji and then traced (using the Scholl Analysis plugin) to gain a much better view of the dendritic arbour and overall morphology of filled neurons (**B**$_2$).*

In some instances, experiments began within minutes of attaining whole-cell configuration, whilst other experiments started only after an extended 20-minute delay (see details below). Recordings were obtained using a MultiClamp 700B amplifier (Molecular Devices, USA), filtered at 10 kHz and digitized at 20 kHz (Axon Digidata 1550A, Molecular Devices, USA) using either WinLTP (WinLTP Ltd.) or Clampex (Molecular Devices Inc.) for storage on the computer hard drive. All electrophysiological experiments were conducted in current clamp mode, where the membrane potential of the cell was free to vary, and any activity recorded was from the neuron's own excitability. Bridge balance was adjusted and monitored regularly throughout every experiment. Additionally, recordings were made in reference to a single AgCl ground pellet (E200, 1.5mm D; Harvard Apparatus) positioned in the bath. Cells were rejected for testing if the current required to hold them at or near –70 mV at the start of an experiment was greater than 100 pA or if the cell had a resting membrane potential more positive than –50 mV.

Bath-Applied Dopamine During Micropipette Dialysis

Within minutes of achieving whole-cell configuration, a current-voltage (I-V) test was administered to assess the electro-responsiveness of the recorded cells. This test was conducted with neurons held close to their resting membrane potential (RMP) at –70mV. During the I-V test, the intrinsic excitability of cells was determined by measuring changes in membrane potential following the injection of hyperpolarising and depolarising current steps (from –200 to +140 pA; 500 ms in duration) in ascending 20 pA increments at a frequency of 1 Hz. Experimental protocols were programmed, controlled and monitored using Clampex (Molecular Devices Inc.). Immediately following the initial I-V test, suprathreshold current was injected (0 to 100 pA) to depolarise neurons to a membrane potential that elicited continuous spiking activity (usually between –50 and –40 mV). The effects of dopamine on the excitability of superficial layer projection neurons in the lateral entorhinal cortex were assessed by monitoring drug-induced changes in holding potential and action potential firing frequency during a period of gap-free recording lasting for 21 minutes (see **Figure 7** below). Following a one-minute baseline period, either ACSF, vehicle (50 µM sodium metabisulfite) or dopamine (100 µM) was added to the perfusate and bath-applied for 5-minutes. The effects of the treatment were then monitored for an additional 15 min of washout. Following the gap-free recording, a second I-V test was conducted at the end of the experiment at –70 mV and later compared to the baseline I-V test (see **Figure 7**).

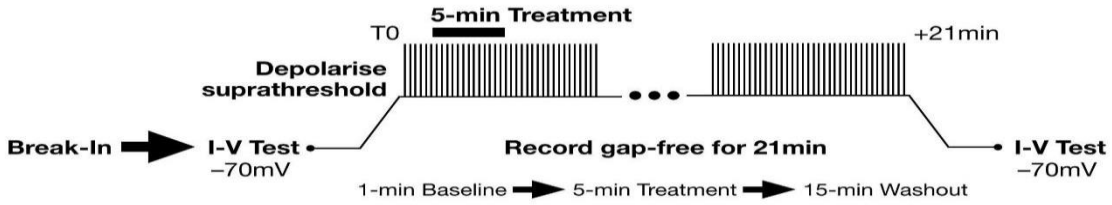

Figure 7. Summary of the gap-free recording protocol performed during micropipette dialysis. *Following break-in, an initial I-V test conducted at –70 mV, and cells were depolarised by direct current injection to a suprathreshold membrane potential sufficient to induce tonic firing. Spiking was monitored before, during and after bath application of various treatments for a period of gap-free recordings lasting 21 minutes. A*

second I-V test was performed at the end of the experiment at –70 mV.

Bath-Applied Dopamine After Micropipette Dialysis

During whole-cell recording experiments, the contents of the intracellular recording micropipette dialyse slowly into patched neurons and eventually reach equilibrium with the intracellular milieu. This is advantageous as it can be leveraged to introduce membrane-impermeable drugs or chemical dyes and tracers directly into the interior of recorded cells. However, there is evidence to show that neuronal excitability may be disrupted during this initial period of dialysis and ionic equilibrium (Davie *et al.*, 2006; Segev, Garcia-Oscos and Kourrich, 2016), and there is washout of key intracellular signals required for some physiological processes, like long-term synaptic potentiation (Simons *et al.*, 2012). As such, an additional set of experiments was conducted in the same manner as those described above, but with the exception that testing was delayed by 20 minutes after the initial break-in to allow this dialysis and stabilisation to occur. During the delay, neurons were maintained near rest at –70 mV.

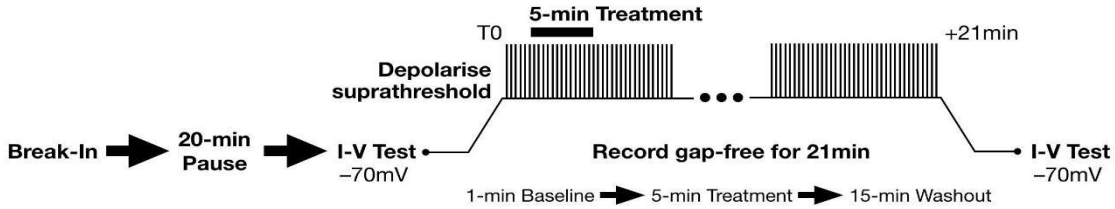

Figure 8. Summary of the gap-free recording protocol performed after micropipette dialysis. *These experiments were identical to those described above and highlighted in* ***Figure 7****, with the exception that there was a 20-min delay after initial break-in prior to starting the experiment to allow for dialysis of the micropipette.*

Pressure-Applied Dopamine onto Individual Neurons

In the experiments described above, dopamine was applied slowly to brain slices for an extended period of time (for 5 minutes) by adding it directly to the perfusate. However, in this set of experiments, dopamine was applied both rapidly *and* transiently by 'puffing' it directly on to individual neurons in the lateral entorhinal cortex via pressure-injection. To achieve this, a borosilicate glass electrode (pulled from 1.2 mm OD glass; Warner Instruments) was pre-loaded with either ACSF, vehicle (50 µM sodium metabisulfite) or dopamine (100 µM) and attached to a microinjector (PV820 Pneumatic PicoPump, World Precision Instruments) placed within 75 µm of the soma of visualised neurons. The pressure injector was positioned first, and then the neuron was patched with a second glass recording micropipette according to the procedures described above. Once whole-cell configuration was achieved, cells were maintained at –70 mV for 20 minutes to allow dialysis to occur. During the experiment, cells were held initially at –70 mV for one minute and then depolarised by delivery of a suprathreshold current step (0 to 140 pA) to a membrane potential sufficient to initiate continuous spiking (-62 to -42 mV for all conditions; see **Figure 9**). The intensity of the current required to initiate spiking was different for each cell, and this was determined in advance just prior to the start of the experiment. The depolarising current step was delivered for a total of three minutes, but at one minute into its delivery, either ACSF, vehicle or dopamine was 'puffed' on to the cell for 100 ms (using N_2 gas delivered at 1 psi to the injection pipette via the PicoPump control unit), and the effects of this treatment on spiking activity monitored for the remaining two minutes of the step. Spiking activity stopped at the offset of the current step when the membrane potential was returned to –70 mV for a final minute of recording. The timing and delivery of both the current step and the synchronised pressure

injection was controlled by WinLTP. Specifically, a TTL signal was delivered by WinLTP via a BNC cable connected to the PicoPump to trigger the puff at the specified moment during the step.

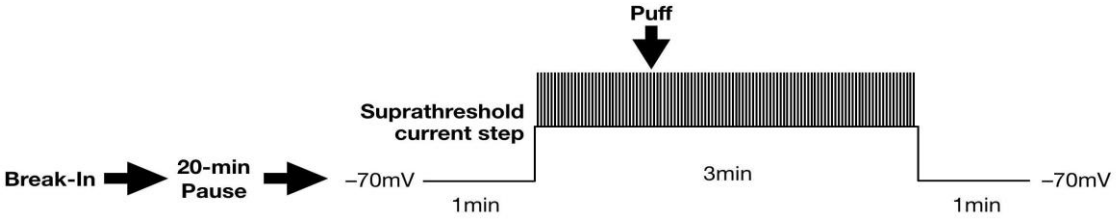

Figure 9. Summary diagram of the pressure-application protocol. *The effects of various treatments on spiking activity was assessed during delivery of a suprathreshold current step lasting 3 minutes. The 100 ms 'puff' was delivered by a nitrogen gas pressure injection at 1-min into the 3-min-long current step.*

II. Perforated Patch Clamp Recordings

The perforated patch clamp method is similar to the standard whole-cell recording techniques described above in that the formation of an initial gigaseal is required. However, this is where the similarities end. In perforated patch clamp recordings, the cell membrane is not ruptured by increased suction, instead an antibiotic is used to 'perforate' the lipid bilayer in order to gain electrical access to the interior of the neuron without going whole-cell (see **Figure 10** below). The microelectrodes used for perforated patch experiments are backfilled with a recording solution containing a concentrated amount of the antifungal and antibiotic compound, nystatin. Nystatin forms pores in the membrane just under the gigaseal by binding to sterols (e.g., cholesterol) located on the surface of the neuronal membrane. Multiple channels are formed that are large enough to permit movement of monovalent ions (e.g., Na^+ and Cl^-) and biocytin molecules across the membrane, yet much too small to allow essential molecules, such as multivalent ions (e.g., Ca^{2+} and Mg^{2+}) and cell organelles, from leaking out (Sarantopoulos, 2007; for review see Ghannoum and Rice, 1999). The perforated patch clamp technique was selected for use here as a way to minimise potential confounds resulting from the dialysis of recorded neurons associated with whole-cell recordings (Davie *et al.*, 2006; Segev, Garcia-Oscos and Kourrich, 2016).

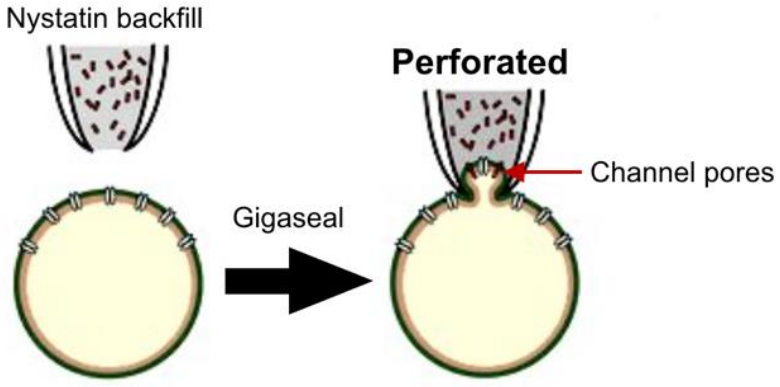

Figure 10. Perforated patch clamp recordings help to minimise confounds associated with micropipette dialysis. *Backfilling recording electrodes with an internal patch solution containing pore-forming antibiotics, like nystatin, permits electrical access without having to go whole-cell. These pores are permeable to small monovalent ions but block dialysis of larger ions and molecules. This maintains the integrity of many cytoplasmic components, including various second messenger systems.*

Recording micropipettes used for perforated patch clamp experiments were loaded with regular whole-cell patch solution (contents listed above) and then backfilled at the tip with patch solution

containing 200 µM nystatin (Fisher Scientific). Concentrated nystatin was stored in the dark at –20 °C and prepared fresh as required. Any nystatin remaining at the end of the test day was discarded. Experiments began as soon as perforated patch configuration was achieved, and this occurred roughly 20 minutes after formation of a gigaseal. This was confirmed by the appearance of fast capacitive transients in the current recording in response to a 10 mV voltage step observed during the seal test (Ishibashi, Moorhouse and Nabekura, 2012; Lucas and Armstrong, 2015). For this experiment, the intrinsic excitability of neurons in the superficial layers of the lateral entorhinal cortex was monitored over an extended period of time. This was achieved by conducting an I-V test once every 5-min for one hour. The protocol for the I-V test used here was identical to the one described above for whole-cell recordings, with the exception that each test here was performed at the natural resting membrane potential of the neuron (-67 to -45 mV for all conditions). After a 10-min baseline period, either ACSF, vehicle (50 µM sodium metabisulfite) or dopamine (100 µM) was bath applied for 10 minutes, and excitability was monitored for an additional 40 minutes during washout (see **Figure 11**).

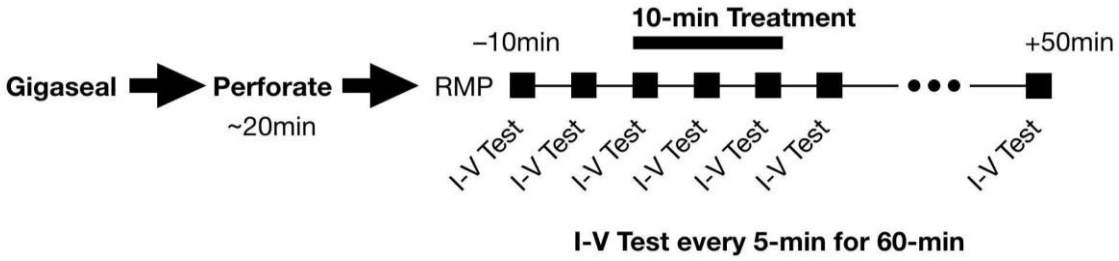

Figure 11. Summary diagram of the perforated patch clamp protocol. *The intrinsic excitability of superficial layer projection neurons in the lateral entorhinal cortex was monitored by delivering an I-V test at rest once every 5 minutes for 60 minutes before, during and after bath-application of various treatments.*

Dopamine Hydrochloride

Dopamine is extremely light sensitive and oxidises rapidly (see **Figure 12** below) so several steps had to be taken to mitigate these effects whenever it was used. Firstly, ambient lighting was reduced in the laboratory during both the preparation and application of dopamine, including for a short period of time after each experimental treatment (for at least 30 min). Additionally, all beakers and tubing used for dopamine experiments were wrapped in foil to block exposure to light. Secondly, the antioxidant, sodium metabisulfite, was added to the final dopamine solutions to help slow oxidation. These methods have been used previously to help maintain the viability, potency and reliability of dopamine during slice recording experiments (Pralong and Jones, 1993; Stenkamp, Heinemann and Schmitz, 1998; Caruana *et al.*, 2006; Rosenkranz and Johnston, 2006; Caruana and Chapman, 2008; Glovaci, Caruana and Chapman, 2014). Dopamine hydrochloride was stored in the dark at 5 °C and prepared fresh as a concentrated stock solution *each and every time it was needed* for an experiment. During preparation, an initial 2 mM stock solution was prepared by first diluting dopamine hydrochloride in ACSF. A number of serial dilutions – also in ACSF – were then performed to reach the desired concentration (100 µM), and sodium metabisulfite (50 µM) was added to this final dopamine solution for use in an experiment.

Figure 12. Dopamine is light sensitive and oxidises rapidly. *In order to slow the oxidation of dopamine once it has been dissolved in solution, the antioxidant sodium metabisulfite (50 µM) is added to slow this process considerably. The beaker on the left contains a 2 mM stock solution of dopamine in ACSF without an antioxidant. Note the black appearance resulting from the oxidation of dopamine. The beaker on the right, however, contains the same stock solution of dopamine, but with 50 µM sodium metabisulfite*

added. Note that the beakers have been wrapped with foil to reduce light exposure.

Labelling and Anatomical Experiments

I. Biocytin-Streptavidin Labelling

The majority of neurons used for the electrophysiological experiments described above were *also* loaded with biocytin (5 mg/mL included in the patch recording solution) in order to label recorded neurons and determine both their overall morphology and precise location in the superficial layers of the lateral entorhinal cortex. Immediately following a recording experiment, slices were placed in a well plate and submerged in 4% paraformaldehyde (PFA) and left at 4 °C in the dark for 12 to 24 hours. Next, slices were washed three times in 4% phosphate buffered saline (PBS; Fluka) and then incubated in a solution containing 4% PBS, 1% Triton X-100 and 0.2% streptavidin (Alexa Fluor 594 (red) and 488 (green) conjugates, Invitrogen) and stored at 4 °C in the dark for 18 hours. Slices were then washed three more times in 4% PBS and mounted on microscope slides using Antifade Mounting Medium with DAPI (Vectashield; Vector Laboratories) and coverslipped. Fluorescent conjugates of streptavidin are used to detect biotinylated molecules, such as biocytin, in order to amplify their signals and make them easy to visualise using a fluorescent microscope.

Slides were imaged using a fluorescent microscope (Eclipse 80i; Nikon) fitted with a CCD monochrome camera (ORCA 285 C4742-96-12G04; Hamamatsu), and neurons were visualised using either a 10x (for neurons with large dendritic arbours) or 40x (for neurons with much smaller dendritic trees) objective. Specialised imaging software (NIS-Elements; Nikon) was used to enhance and then capture images of the visualised neurons, and the files were saved to the computer hard drive in both ND2 and JPG formats. Additionally, a series of images (≤ 70) along the z-axis was captured at 5 µm intervals through each slice and saved as either an AVI video file or a compressed JPEG image file.

II. Tyrosine Hydroxylase Immunohistochemistry

Horizontal slices of the hippocampal formation and parahippocampal cortices not used for electrophysiological recording work were utilised for experiments to assess the density and distribution of tyrosine hydroxylase-positive fibres across the laminar extent of the lateral entorhinal cortex. A hydrophobic pen (ImmEdge Hydrophobic Barrier PAP, H-4000; Vector Laboratories) was used to delineate borders on microscope slides to isolate individual slices for immunolabeling work. Slices were positioned in the centre of each bordered region in the same orientation and then treated with a blocking solution consisting of (in mM): 0.1 normal goat serum, 0.01 Triton X-100 and 0.98 PBS. Slices were then left on a rotator for two hours. Following several PBS rinses to remove the blocking solution, slices were incubated in primary antibody (rabbit anti-TH, 1:1000 dilution; AB152, Millipore) for 3 days at 4 °C. Following a series of washes in PBS, the slices were incubated for 3 additional hours in secondary antibody (goat anti-rabbit with Alexa 480, 1:500 dilution; AB150077, Abcam). After a final series of PBS washes, a drop of Vectashield was applied to each slice and a coverslip positioned on the slides.

Data Analysis

Electrophysiology data were analysed using Clampfit (Molecular Devices), AxoGraph X (AxoGraph

Scientific) and Microsoft Excel (Microsoft Corporation). Data were plotted and visualised using GraphPad Prism (GraphPad Software Inc.), and Prism was used for all statistical analyses described below. Images were compiled and catalogued in Adobe Lightroom (Adobe Inc.), and all image processing and analysis was performed in Fiji (open source version of ImageJ). Quantified image data were compiled in Excel and both plotted and analysed using Prism. Final Figures were prepared in Adobe Illustrator (Adobe Inc.).

I. Whole-Cell Patch Clamp Data Analysis

The intrinsic excitability of neurons was assessed by counting the number of spikes evoked in response to 500 ms-duration suprathreshold depolarising current steps (0 to +140 pA in ascending 20 pA increments) from a constant holding potential (typically –70 mV). Input resistance was calculated by measuring both the peak and the steady-state voltage responses to −200 pA current steps (500 ms in duration), and inward rectification was quantified by expressing the peak input resistance as a proportion of the steady-state resistance (rectification ratio). All data were expressed as the mean ± SEM for plotting, and changes in response properties before and after each gap-free experiment were assessed using paired samples t-tests or repeated measures ANOVAs.

To assess changes in neuronal excitability during gap-free recordings, the number of spikes elicited by constant suprathreshold current injection was assessed in 1-min bins observed during the baseline period, the first minute post-treatment and the penultimate minute of the experiment during washout (see **Figure 15A$_1$**). The number of spikes per bin were normalised to spiking levels observed during the baseline period and expressed as the mean ± SEM for plotting. Changes in neuronal excitability during the experiment and across treatment conditions were assessed using repeated measures ANOVAs and Bonferroni post hoc tests.

During pressure injection experiments, a suprathreshold current step was sufficient to induce tonic spiking in superficial layer projection neurons in the lateral entorhinal cortex. The number of spikes elicited by the step were counted and binned into 5-second epochs and then averaged across cells. The average number of spikes per bin were expressed as the mean ± SEM for plotting, and the entire cohort of recorded cells was then analysed together, as well as for layer II and layer III, individually. Changes in the number of action potentials elicited by the 'puff' were assessed by comparing pre-puff spiking (the average of the last two bins just prior to the puff) to post-puff spiking (the single bin 10-sec post-puff) for each treatment condition. Data were averaged and plotted as box and whisker plots and compared using paired samples t-tests.

II. Perforated Patch Clamp Data Analysis

Changes in the intrinsic excitability of superficial layer projection neurons in the lateral entorhinal cortex were assessed by administering an I-V test once every 5 min for 60 minutes (see **Figure 11** above), and key measures were compared before and after each treatment. A number of separate analyses were performed on data collected during each I-V test. The intrinsic excitability of projection neurons was assessed by counting the number of spikes elicited in response to 500 ms-duration suprathreshold depolarising current steps (0 to +140 pA in ascending 20 pA increments) from a constant holding potential (the natural RMP of the cell) and plotted as input-output curves before and after each treatment. RMP was recorded at the start of each I-V test and monitored throughout the entire experiment. Spiking activity was assessed every 5 minutes during the 60-min experiment using the lowest intensity current step (from the I-V test) required to trigger at least 5 action potentials during the baseline. Input resistance was calculated by measuring both

the peak and the steady-state voltage responses to −200 pA current steps (500 ms in duration), and inward rectification was quantified by expressing the peak input resistance as a proportion of the steady-state resistance (rectification ratio). All data were expressed as the mean ± SEM for plotting, and changes in response properties were assessed before and after treatment using repeated measures ANOVAs. Post hoc comparisons were made using the Bonferroni method with the alpha level set to $P < 0.05$. All analyses were performed on pooled data, as well as on smaller subsets in which data for layer II cells and layer III cells were collated separately.

Image Analysis for Tyrosine Hydroxylase Immunohistochemistry

A fluorescein isothiocyanate (FITC) green filter illuminated the tyrosine hydroxylase immunolabelling in slices containing the lateral entorhinal cortex, and images were taken at low magnification (1x) in order to show the location of the lateral entorhinal cortex in each slice. Next, a series of roughly 70 images were taken at a higher 4x magnification along the z-axis in 5 µm intervals to capture the distribution of fibres throughout each slice. These images were then processed and analysed using Fiji by flattening each z-stack to create a single focussed image containing fluorescent data for the entire lateral entorhinal cortex (see **Figure 13A$_1$**). Images were then converted into 8-bit grayscale format. A large background signal was produced in each focussed image as a by-product of the flattening process and the 'subtract background' algorithm in Fiji was used to reduce this significantly (see **Figure 13A$_2$**). All images (from the same animal) were then enhanced using the same settings to optimise the fluorescent signal and make it brighter (see **Figure 13A$_3$**). Adopting anatomical data from Ray and Brecht (2016) as a guide, a single-pixel line 1400 µm in length was drawn across each cortical layer starting from the surface (layer I) and ending in the deep layers of the lateral entorhinal cortex (layers V-VI; see **Figure 13B$_1$**). This line served to ensure that the regions of interest (ROIs, see below) required for analysis were positioned correctly within the centre of each cortical layer. Enhanced images were then binarised to obtain brightness values between 0 and 255 (white-to-black) by global thresholding. To clearly show the extent of tyrosine hydroxylase labelling, autothreshold was used in Fiji, inverting the image as shown in **Figure 13B$_2$**. Then 100 µm² ROIs were drawn in the middle of each layer along the 1400 µm-long pre-specified path (see **Figure 13C**). The mean gray value for each ROI was measured in Fiji, giving an estimate of the intensity of the fluorescence signal within the sampled region. The intensity of fluorescence in each layer was then expressed as a percentage of the total fluorescence measured. Data were plotted as mean ± SEM and analysed across layers using a one-way ANOVA and Bonferroni post hoc comparisons.

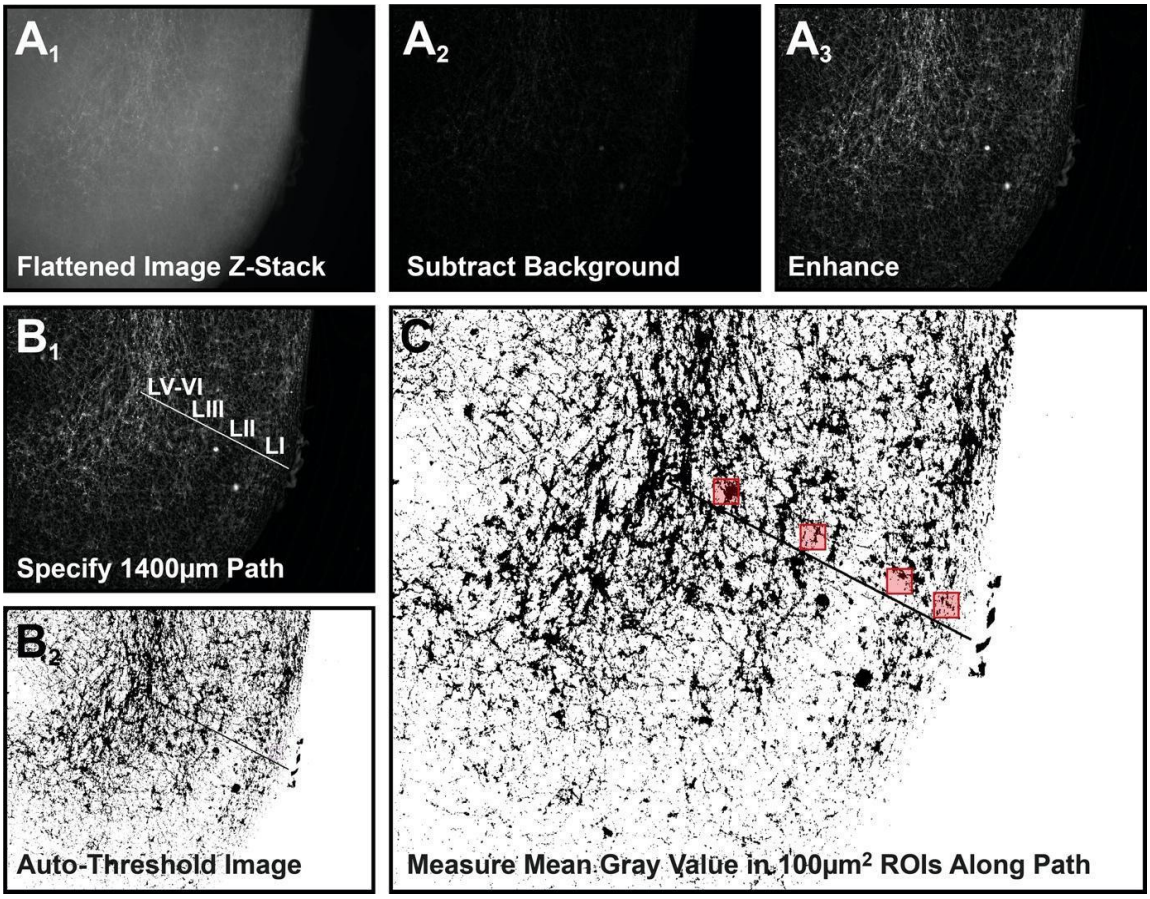

Figure 13. Summary of the steps involved in the analysis of images showing the expression and distribution of TH-positive fibres in horizontal slices of the lateral entorhinal cortex. *A series of up to 70 images were captured at 5 µm intervals through each slice. These images were flattened into a single representative plate (**A_1**), had the background subtracted (**A_2**) and were enhanced digitally to visualise the immunolabelling (**A_3**). Next, a 1400 µm path was specified spanning each layer of the lateral entorhinal cortex (**B_1**), and auto-thresholding was used to better visualise the distribution of labelling in the slice (**B_2**). Finally, a 100 µm^2 region of interest (ROI) was specified in the middle of each cortical layer, and the mean gray value was measured in each ROI to estimate the density of fluorescent labelling in each cortical layer (**C**).*

RESULTS

The Distribution of Tyrosine Hydroxylase-Positive Fibres in the Lateral Entorhinal Cortex

Immunolabeling for tyrosine hydroxylase was used to determine the expression pattern of dopaminergic fibres in the lateral entorhinal cortex. This method facilitates the visualisation of neurons that contain tyrosine hydroxylase, a rate limiting enzyme required for the biosynthesis of catecholamines, including dopamine. Indeed, antibodies against tyrosine hydroxylase have been used previously on tissue from humans (Akil and Lewis, 1994), rodents (Mingote *et al.*, 2015) and primates (Akil and Lewis, 1993) to map patterns of dopaminergic innervation in the hippocampal formation and parahippocampal cortices. Here, tyrosine hydroxylase-positive fibres were labelled successfully in 340 µm-thick horizontal slices (from P14 to P21 rats) containing the lateral entorhinal cortex, and this allowed for specific patterns in fibre innervation to be observed (See **Figure 14A$_1$**). In particular, expression was high in both the superficial (**Figure 14A$_2$**) and deep layers (**Figure 14A$_3$**) of the lateral entorhinal cortex. This is clearly visible in the 'banded' appearance of the tyrosine hydroxylase-positive fluorescent labelling across each cortical layer (see **Figure 14B$_2$**).

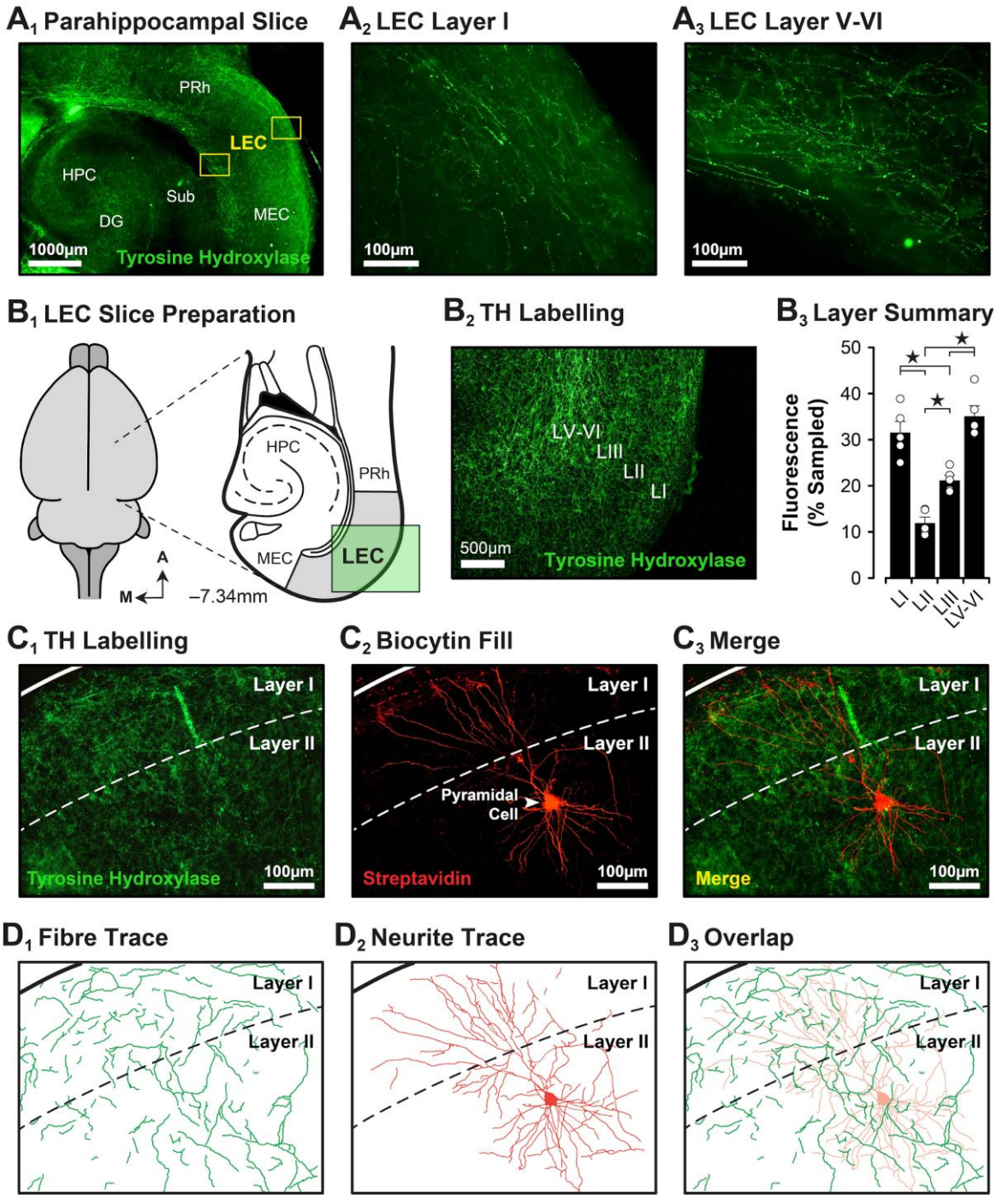

Figure 14. Pattern of tyrosine hydroxylase immunolabelling in the lateral entorhinal cortex. *Horizontal slices not used for electrophysiological recordings were processed for tyrosine hydroxylase (TH) immunoreactivity instead. TH-positive fibres were expressed throughout the slices, including in the hippocampus (HPC), dentate gyrus (DG), perirhinal cortex (PRh), and in both the medial and lateral entorhinal cortices (MEC and LEC, respectively;* ***A1****). Expanded views of boxed regions in* ***A1*** *highlight the density of TH-positive fibres located in layer I (****A2****) and in layers V-VI (****A3****). The pattern of expression of TH-positive fibres was quantified and compared across each cortical layer. Schematic diagram in* ***B1*** *highlights an expanded view of the horizontal slice preparation indicating the region of the lateral entorhinal cortex selected for analysis (green box). There was a distinct pattern in the expression of TH-positive fibres across cortical layers, and this is seen clearly in the 'banded' appearance of the fluorescent labelling in flattened and enhanced z-stack images (****B2****). A summary bar plot highlighting differences in the amount of fluorescence measured across layers in the lateral entorhinal cortex (mean ± SEM in this and subsequent Figures) is shown*

*in **B_3** (⋆ indicates P < 0.05). Some slices were double labelled for tyrosine hydroxylase (**C_1**) and streptavidin (**C_2**) to assess the overlap (**C_3**) between dopaminergic fibres and projection neurons in the superficial layers. Images in **D** show trace reconstructions of the fibres and neurites shown in the corresponding images in **C**.*

Indeed, there was a significant difference in the distribution of fluorescent labelling across the entire laminar extent of the lateral entorhinal cortex ($F_{3,16}$ = 33.06, P < 0.0001; see **Figure 14B$_3$**; n = 5 animals, multiple slices per brain, pooled). Specifically, expression was highest in superficial layer I and in deep layers V-VI (31.6 ± 2.4% of total fluorescence sampled for layer I and 35.1 ± 2.2% of total fluorescence sampled for layers V-VI), followed next by layer III (21.2 ± 1.1% of total fluorescence sampled), and then by layer II (12.0 ± 1.2%of total fluorescence sampled). Interestingly, the amount of fluorescence did not differ significantly between layer I and layers V-VI (Bonferroni, P = 0.53). In other experiments, double labelling for tyrosine hydroxylase and streptavidin (to label biocytin-filled neurons) showed that dopaminergic fibres overlapped significantly with superficial layer projection neurons in the lateral entorhinal cortex (**Figure 14C** and **14D**). Data shown in **Figure 14C** and **14D** highlights overlap in layer I where the apical dendritic trees of principle neurons ramify and make synaptic contact with inputs from sensory cortices, as well as in layer II where the cell bodies of projection neurons reside (see **Figure 14C$_3$** and **14D$_3$**). As such, dopaminergic inputs from the midbrain are well-poised to modulate both the integration of sensory inputs in the lateral entorhinal cortex and the propagation of sensory signals to the rest of the hippocampal formation.

Dopaminergic Modulation of Neuronal Excitability in the Superficial Layers

Gap-Free Recordings During and After Micropipette Dialysis

As shown above, tyrosine hydroxylase fibres are expressed in the lateral entorhinal cortex, including in the superficial layers where the cell bodies of neurons that project to the hippocampus are located. Interestingly, the distribution pattern of these fibres is layer-specific with denser innervation occurring in layer III than in layer II. This suggests, therefore, that dopamine may module layer III neurons differently from those found in layer II. Indeed, little is known about how dopamine modulates the intrinsic excitability of superficial layer projection neurons in the lateral entorhinal cortex (but see Caruana and Chapman, 2008; Batallán-Burrowes and Chapman, 2018) or whether this modulation differs depending on cortical layer.

Initial experiments were performed to assess the effects of bath-applied dopamine on the spiking activity of neurons located in the superficial layers of the lateral entorhinal cortex. During these experiments, slow injection of positive current was used to depolarise neurons above threshold to trigger continuous action potential discharges. The number of spikes fired was then monitored during a period of gap-free recording lasting for 21 minutes before, during and after 5-min bath application of either ACSF (control; n = 3), vehicle (50 µM sodium metabisulfite; n = 5) or dopamine (100 µM; n = 2). Spiking during 1-min epochs recorded at different times during the experiment (baseline, post-treatment, and washout) were normalised to baseline levels and compared. Additionally, given the small sample size, data for all superficial layer neurons (recorded from both layers II and III) was pooled. Interestingly, there was no significant effect of any treatment on spiking activity in superficial layer neurons (Mixed-effects model, P = 0.55; see **Figure 15A$_{1-4}$**). The most robust effects on spiking were observed following bath-application of dopamine (see **Figure 15A$_3$**). Although not significant, the pattern of activity was somewhat consistent in that all treatments appeared to reduce spiking during the 5-min period of bath-application, as well as for a short period of time during washout. Treatment with sodium metabisulfite (50 µM) has been shown previously to have no effect on synaptic transmission in the lateral entorhinal cortex (Caruana *et al.*, 2006; Caruana and Chapman, 2008; D Caruana unpublished observation) so it is

surprising that it appeared to affect neuronal activity here (**Figure 15A$_2$**). It is also surprising that standard ACSF reduced spiking in a manner similar to vehicle (**Figure 15A$_1$**). These findings suggest, therefore, that something other than treatment condition alone may be influencing the results observed here.

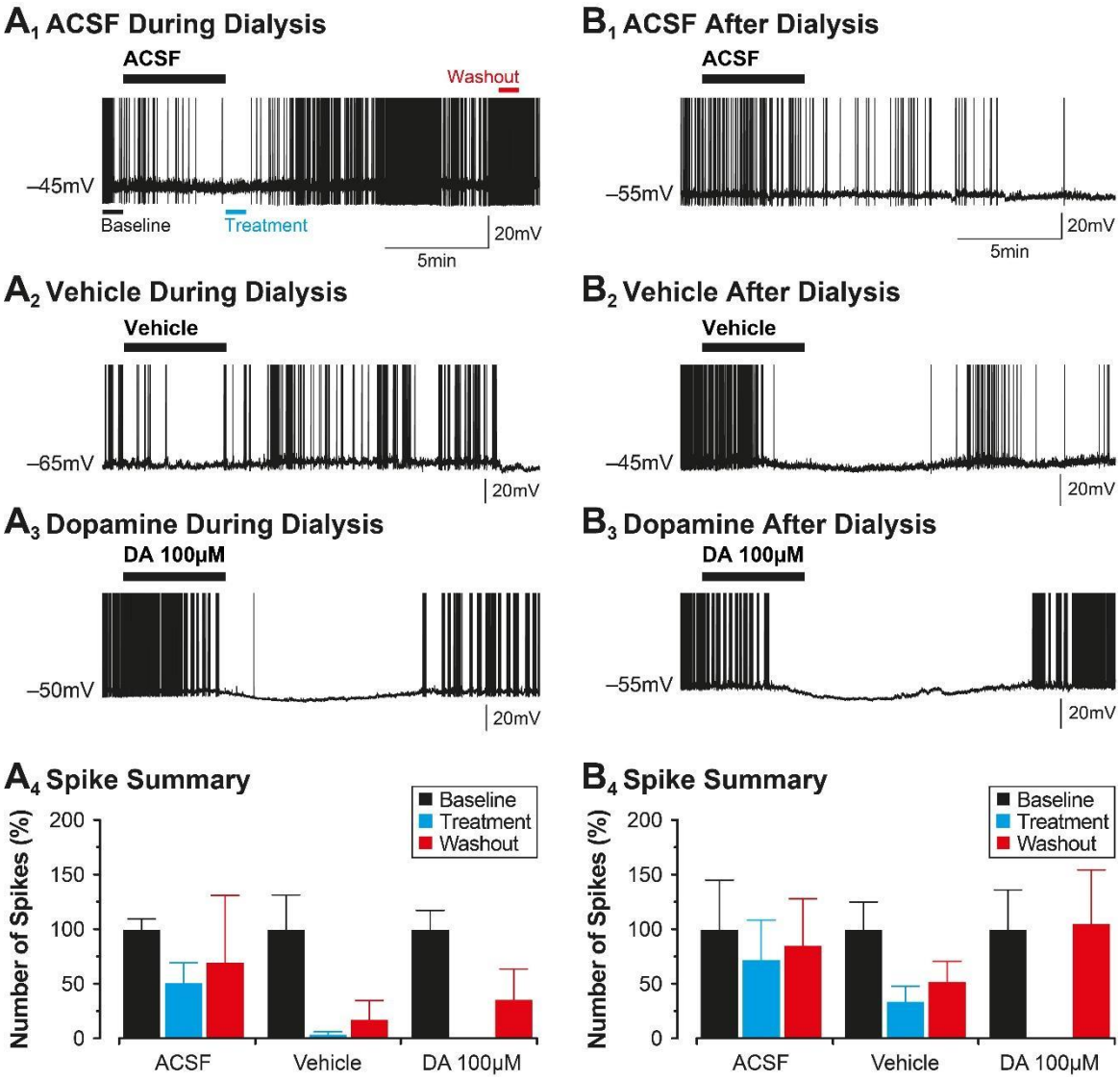

Figure 15. Bath-applied treatments have variable effects on spiking activity in superficial layer projection neurons. *Gap-free recordings started within minutes of breaking into the cells highlight the variable effects different treatments have on spiking activity in principal neurons in the lateral entorhinal cortex (**A**). The number of action potentials elicited by neurons depolarised by suprathreshold current injection is reduced during and after bath-application of either ACSF (**A$_1$**) or 50 µM sodium metabisulfite (Vehicle; **A$_2$**). Application of dopamine also reduced spiking (**A$_3$**) in a more reliable manner. Also note the change in membrane potential (V_m) during washout elicited by dopamine in **A$_3$**. Interestingly, spiking recovered, at least in part, towards the end of washout. Pooled data in **A$_4$** highlights the average number of spikes (mean ± SEM) elicited during 1-min bins sampled at different times during the experiment (indicated by the horizontal bars in **A$_1$**). The coloured bars in **A$_4$** correspond to the matching coloured lines shown in **A$_1$** to indicate the time points compared during gap-free experiments. A similar pattern is observed in data shown in **B** in which identical experiments were performed in separate groups of cells following a 20-min delay after initial break-in.*

To determine whether micropipette dialysis contributed to the variable effects on spiking activity observed following the array of bath-applied treatments, the same experiments were repeated on a different cohort of superficial layer neurons, but experiments began only after a 20-min delay to allow dialysis and ionic equilibrium to occur after the initial break-in (see **Figure 15B**). Once again, neurons were depolarised above threshold and the number of spikes fired was monitored during a period of gap-free recording (21-min in duration) before, during and after 5-min bath application of either ACSF (control; n = 7), vehicle (50 µM sodium metabisulfite; n = 7) or dopamine (100 µM; n = 6). Again, there was no significant effect of any treatment on spiking activity in superficial layer neurons (see **Figure 15B$_{1-4}$**). Indeed, a general trend showed a reduction in spiking during and after bath-application, with the most pronounced effects induced by dopamine, but these effects were variable and not significant (Mixed-effects model, P = 0.61; see **Figure 15B$_4$**). These findings suggest that dopamine could potentially have a suppressive effect on the excitability of superficial layer projection neurons in the lateral entorhinal cortex, and that other factors related to the recording method or preparation of the various treatments may partially occlude the results.

Pressure-Application of Dopamine Directly to Individual Superficial Layer Neurons

As noted above, there is evidence to suggest that dopamine may reduce the excitability of superficial layer projection neurons in the lateral entorhinal cortex by attenuating spiking activity, and that other factors may be involved. In the next set of experiments, the amount of time in which whole-cell recordings were performed, including the amount of time in which the various treatments were applied, were both reduced considerably. In addition, treatments were applied directly to individual neurons via pressure injection in order to limit overall exposure, as well as to minimise changes in any local inhibitory network activity that may also be affected when applying treatments to the entire slice simultaneously.

During the pressure-application experiments, cells were depolarised by a suprathreshold current step from a holding potential of –70 mV to induce continuous spiking activity. The depolarising step lasted for 3-min, but at 1-min into the depolarising current step, a 100 ms 'puff' of either ACSF (n = 11), 50µM sodium metabisulfite (Vehicle; n = 11) or dopamine (100 µM; n = 10) was applied via pressure injection at 1 psi (see **Figure 16A$_{1–2}$**) and the effects on spiking monitored during the reminder of the step (see **Figure 16A$_3$** for schematic summary). Initially, effects of the various treatments on spiking were assessed on pooled data for all neurons tested (cells in layers II and III combined). Focal application of ACSF via pressure injection had no significant effect on spiking activity, nor did treatment with vehicle (**Figure 16B$_1$** and **16C$_1$**, respectively) on pooled data. Averaged spiking measured during the 5-sec bin at the 10-sec post-puff time point did not differ significantly from the pre-puff baseline (ACSF: pre-puff 4.9 ± 1.1 spikes, post-puff 5.2 ± 1.6 spikes; t_{10} = 0.26, P = 0.80; **Figure 16B$_4$** All Cells; Vehicle: pre-puff 7.3 ± 1.2 spikes, post-puff 6.7± 2.7 spikes; t_{10} = 0.33, P = 0.75; **Figure 16C$_4$** All Cells). This stability suggests that cells were not affected in an adverse manner by any mechanical factors associated with the puff (i.e., puff-induced movement/disruption of cells), nor by the control treatments themselves. Similarly, pressure injection of dopamine also had no significant effect on spiking in the pooled dataset, though a general trend towards a reduction in the number of action potentials elicited following the puff was observed (pre-puff 9.1 ± 3.3 spikes reduced to 3.3 ± 1.5 spikes post-puff; t_9 = 1.59, P = 0.15; see **Figure 16D$_1$** and **16D$_4$** All Cells).

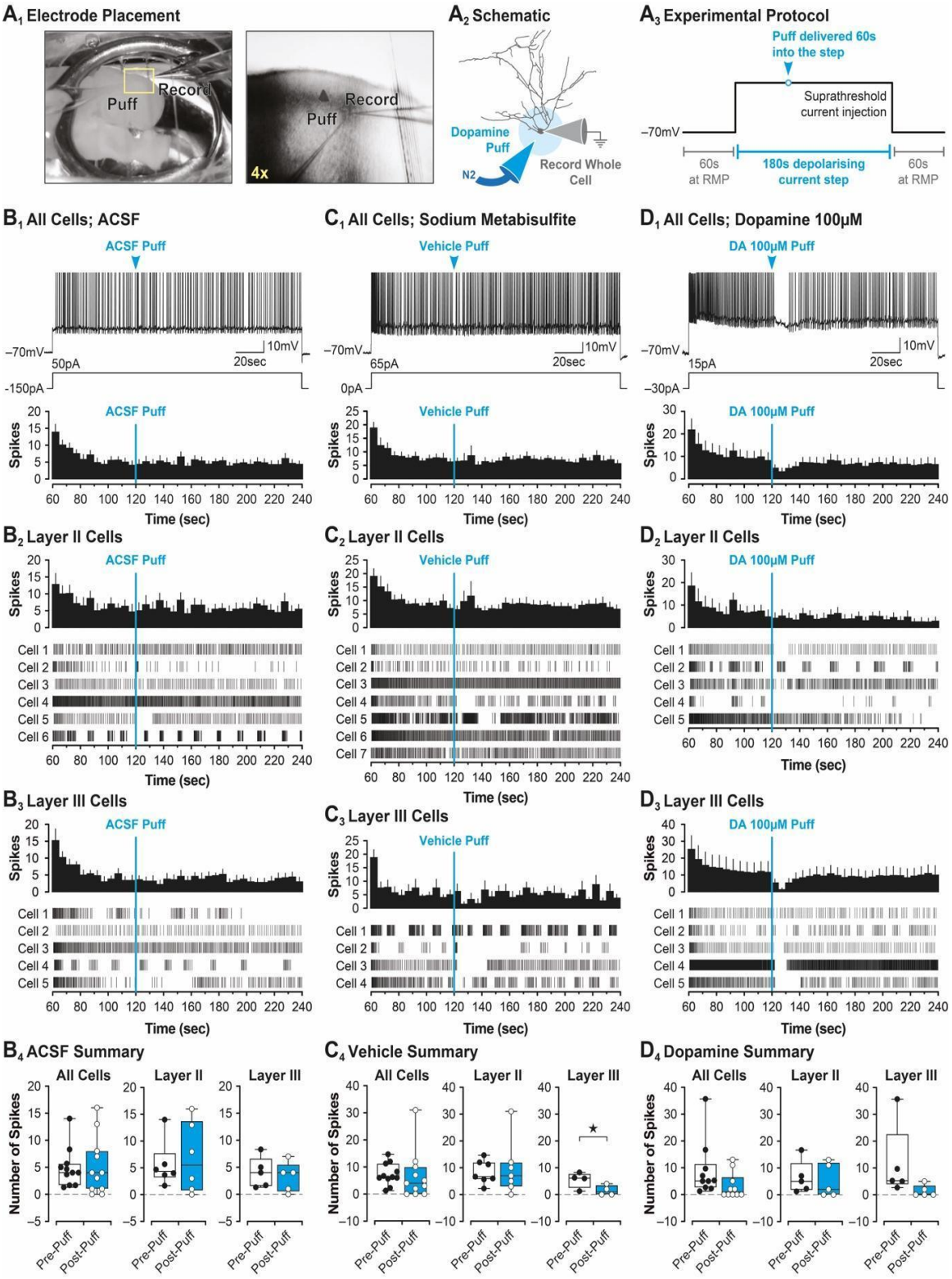

Figure 16. Dopamine applied directly to individual neurons via pressure injection reduces spiking selectively in layer III neurons. *A glass micropipette filled with either ACSF, sodium metabisulfite (50 µM) or dopamine (100 µM) was positioned close to the soma of patched neurons, and nitrogen gas was used to briefly 'puff' the treatments directly on to cells during an experiment. The image on the left in* ***A₁*** *shows a wide view of the orientation and position of both the injection (Puff) and patch (Record) electrodes relative to a horizontal brain slice. The right image shows an expanded 4x view of the same electrodes (cropped to the yellow boxed region). A schematic representation of micropipette orientation relative to a single traced*

*neuron is shown in **A_2**. For these experiments, a 100 ms 'puff' was used to deliver drugs directly to individual cells. This puff was delivered at 1-min into a 3-min depolarising current step as outlined in the protocol shown in **A_3**. The effects of pressure-applied drugs on spiking activity is shown in the representative traces displayed along the top (action potentials have been truncated) for ACSF (**B_1**), sodium metabisulfite (**C_1**) and dopamine (**D_1**), and pooled summary data for all superficial layer projection neurons is shown below each trace. Note: The number of spikes elicited by the step were counted and binned into 5-second epochs and then averaged across cells within each condition. Arrows above the traces and the lines dissecting the summary bar plots indicate the time points when the 'puff' was delivered. Data shown in **B_2**, **C_2** and **D_2** are for the ACSF, vehicle (50 µM sodium metabisulfite) and dopamine (100 µM) treatment conditions, respectively, but only for neurons located in Layer II. Conventions for the summary bar plots are the same as in **B_1**, **C_1** and **D_1**. Below the pooled data are individual records showing the spike activity for each neuron included for analysis. Note: Vertical lines indicate spikes (1 vertical line = 1 action potential) as well as the latency when the spikes occurred during the current step. Spiking activity for Layer III neurons is shown in **B_3**, **C_3** and **D_3** for the ACSF, vehicle and dopamine conditions, respectively. Conventions are the same as for Layer II cells. Treatment-induced changes in spiking were compared before (Pre-Puff) and 10 sec after (Post-Puff) the pressure injection, and data are shown as box and whisker plots for ACSF (**B_4**), vehicle (**C_4**) and dopamine (**D_4**), respectively. For each condition, pooled data for all superficial layer cells is shown on the left (All Cells), Layer II data in the middle, and Layer III data on the right (* indicates $P < 0.05$).*

To assess whether dopamine had differential effects on layer II versus layer III neurons, the pooled data were separated, and spiking activity was analysed independently for each cortical layer. There was no effect of any treatment on spiking activity in layer II neurons (see **Figure 16B$_2$**, **C$_2$** and **D$_2$**). Spiking remained stable post-puff relative to the pre-puff baseline following pressure application of either ACSF (from 5.6 ± 1.8 spikes pre-puff to 6.8 ± 2.7 spikes post-puff; $t_5 = 0.73$, $P = 0.50$; n = 6; **Figure 16B$_4$** Layer II), sodium metabisulfite (from 8.4 ± 1.6 spikes pre-puff to 9.7 ± 3.9 spikes post-puff; $t_6 = 0.50$, $P = 0.63$; n = 7; **Figure 16C$_4$** Layer II), or dopamine (from 6.4 ± 2.7 spikes pre-puff to 5.2 ± 2.8 spikes post-puff; $t_4 = 0.51$, $P = 0.64$; n = 5; **Figure 16D$_4$** Layer II). In layer III neurons, treatment with ACSF also had no effect on spiking (pre-puff 4.2 ± 1.4 spikes, post-puff 4.3 ± 1.4 spikes; $t_4 = 0.72$, $P = 0.61$; n = 5; **Figure 16B$_4$** Layer III), but there was a reduction in the number of action potentials observed following pressure application of sodium metabisulfite (spiking reduced post-puff to 1.5 ± 1.0 spikes from 5.5 ± 1.5 spikes pre-puff; $t_3 = 3.89$, $P < 0.05$; n = 4; **Figure 16B$_4$** Layer III). Interestingly, there was also a trend towards a reduction in the number of spikes observed in 4 out of 5 layer III neurons tested following pressure-application of 100 µM dopamine from 11.7 ± 6.1 spikes pre-puff to 1.4 ± 1.0 spikes post-puff (see **Figure 16D$_3$**), though this was not significant ($t_4 = 1.57$, $P = 0.19$; n = 5; **Figure 16D$_4$**). These findings suggest that dopamine may have more selective effects on layer III neurons as opposed to layer II neurons but given the reduction in spiking induced by sodium metabisulfite, these findings should be interpreted cautiously.

Long-Term Monitoring of Neuronal Excitability Using the Perforated Patch Clamp Method

In order to mitigate the effects of micropipette dialysis and to enhance stability when performing long-duration recordings, the perforated patch clamp method was applied. Here, the intrinsic excitability of layer II and layer III projection neurons was monitored at 5-min intervals for one hour. Following successful perforation (taking around 15 minutes after gigaseal formation), and after a 10-min baseline period, either ACSF, vehicle (sodium metabisulfite, 50 µM) or dopamine (100 µM) was bath-applied for 10-min, and excitability monitored for an additional 40-min during washout. Intrinsic excitability was assessed by delivering an I-V test from the natural and uncorrected resting membrane potential of the cell, and changes in spiking, membrane potential (V_m) and input resistance (R_{in}) analysed before (at –5-min) and at peak post-treatment (at +5 or

10-min). Sodium metabisulfite (n = 10), although having displayed some efficacy in previous experiments, was shown to have no effect on excitability measured here (**Figure 17A$_1$**). The number of action potentials elicited in response to a depolarising current step remained stable throughout the entire 60-min recording period (**Figure 17A$_1$** top, filled circles), and there was no change in membrane potential (**Figure 17A$_1$** bottom, filled circles) or input resistance (not shown) observed in the pooled dataset (All Cells). Similarly, bath-application of normal ACSF (n = 10) had no effect on measures of intrinsic excitability (**Figure 17A$_1$** top and bottom, open circles). In addition, the number of spikes elicited by suprathreshold current injection delivered in ascending 20 pA steps (from 0 to +140 pA) was the same before and immediately after 10-min treatment with sodium metabisulfite (see **Figure 17A$_2$**). These results indicate that control treatments had no effect on the intrinsic excitability of superficial layer projection neurons in the lateral entorhinal cortex.

In contrast, bath application of 100 µM dopamine caused a large attenuation in spike activity and membrane potential in the pooled data for all cells tested (n = 12). The number of spikes elicited in response to a fixed-intensity suprathreshold current step was reduced from 5.1 ± 0.1 spikes during the baseline to 3.0 ± 0.6 spikes after treatment with dopamine, and this differed from the number of spikes elicited in time-matched control cells treated with ACSF (5.3 ± 0.2 spikes post-treatment; $F_{1,20} = 11.21$, $P < 0.01$; Bonferroni $P < 0.001$; n = 10; see **Figure 17B$_1$** top). The dopamine-induced attenuation in spiking was also linked to a concurrent change in the membrane potential of the recorded cells. Neurons were hyperpolarised from –54.8 ± 1.3 mV during the baseline to –60.2 ± 1.3 mV following dopamine application, and this differed from time-matched controls (–53.8 ± 1.6 mV post-treatment; $F_{1,20} = 14.65$, $P < 0.01$; Bonferroni $P < 0.01$; see **Figure 17B$_1$** bottom). These effects were transient as both spiking and membrane potential returned to baseline levels within the first 5 to 10 minutes of washout. In addition, dopamine caused a rightward shift in the spike input-output curve indicating that excitability was reduced across a wide range of current intensities tested (see **Figure 17B$_2$**). These data indicate that dopamine has a considerable effect on the intrinsic excitability of superficial layer projection neurons in the lateral entorhinal cortex.

To assess whether dopamine had differential effects on the intrinsic excitability of layer II versus layer III neurons, the pooled data were divided and measures of intrinsic excitability (spikes, V_m and R_{in}) analysed separately. In layer II, bath-application of 100 µM dopamine caused a large reduction in the number of action potentials triggered by suprathreshold current injection (**Figure 17C$_2$** and **C$_3$** top, filled circles; n = 5). Spiking was reduced from an average of 4.8 ± 0.2 spikes during the baseline to 1.8 ± 0.8 spikes after dopamine treatment, and this differed substantially from spiking in time-matched control experiments in layer II neurons treated with ACSF (5.2 ± 0.2 spikes post-treatment; $F_{1,8} = 15.0$, $P < 0.01$; Bonferroni $P < 0.001$; n = 5; see **Figure 17C$_3$** top, open circles). There was also a coincident change in membrane potential that was time-locked to the effects on spiking (see **Figure 17C$_3$** bottom, filled circles). Layer II neurons were hyperpolarised by dopamine from –54.0 ± 1.6 mV during the baseline to –61.6 ± 1.6 mV after treatment, and this differed significantly from the resting membrane potential of time-matched controls treated with ACSF (–51.6 ± 1.5mV post-treatment; $F_{1,8} = 22.56$, $P < 0.01$; Bonferroni $P < 0.001$; see **Figure 17C$_3$** bottom, open circles). Again, these effects were only transient as both spiking and membrane potential returned to baseline levels within the first 5 to 10 minutes of washout. There was also a prominent rightward shift in the spike input-output curve for layer II neurons treated with dopamine (see **Figure 17C$_4$**). The changes in both spiking and membrane potential in layer II neurons mediated by dopamine were also linked to dopamine-induced changes in input resistance (see **Figure 17C$_5$** and **C$_6$**). Input resistance was assessed by measuring both the peak and steady-state changes in membrane potential from rest following injection of a –200 pA hyperpolarising current step (recorded during each I-V test). Peak input resistance is the pure measure of membrane resistance

uncontaminated by any inward rectification, such as the hyperpolarisation-activated nonspecific cation current (I_h), observed during the steady-state. Neurons in the medial entorhinal cortex show pronounced inward rectification mediated by I_h (Giocomo and Hasselmo, 2008; Heys and Hasselmo, 2012), but this rectification is practically non-existent in superficial layer projection neurons in the lateral entorhinal cortex. Here, there was also very little inward rectification observed in layer II neurons, and both peak and steady-state measures of input resistance were attenuated by dopamine relative to controls (Peak: reduced to 74.6 ± 5.6% of baseline; Steady: reduced to 74.8 ± 4.9% of baseline; $F_{3,21}$ = 14.06, P < 0.0001; Peak Bonferroni, P < 0.001; Steady Bonferroni, P < 0.001; see **Figure 17C$_5$** top and **C$_6$**). Interestingly, the effects of dopamine on the intrinsic excitability of superficial layer projection neurons in the lateral entorhinal cortex were much less pronounced on layer III neurons than they were on layer II neurons. Although dopamine caused an attenuation of spiking in layer III neurons relative to controls (spiking reduced from 4.9 ± 0.3 spikes to 3.1 ± 0.4 spikes; $F_{1,10}$ = 10.74, P < 0.01; Bonferroni P < 0.001; n = 7; see **Figure 17D$_3$** top), this was not accompanied any notable change in resting membrane potential (**Figure 17D$_3$** bottom) or input resistance (see **Figure 17D$_5$** and **D$_6$**). These findings indicate that dopamine has both differential and disproportionate effects on the intrinsic excitability of layer II versus layer III neurons in the lateral entorhinal cortex, and that the mechanisms underlying these effects may differ significantly between the two layers.

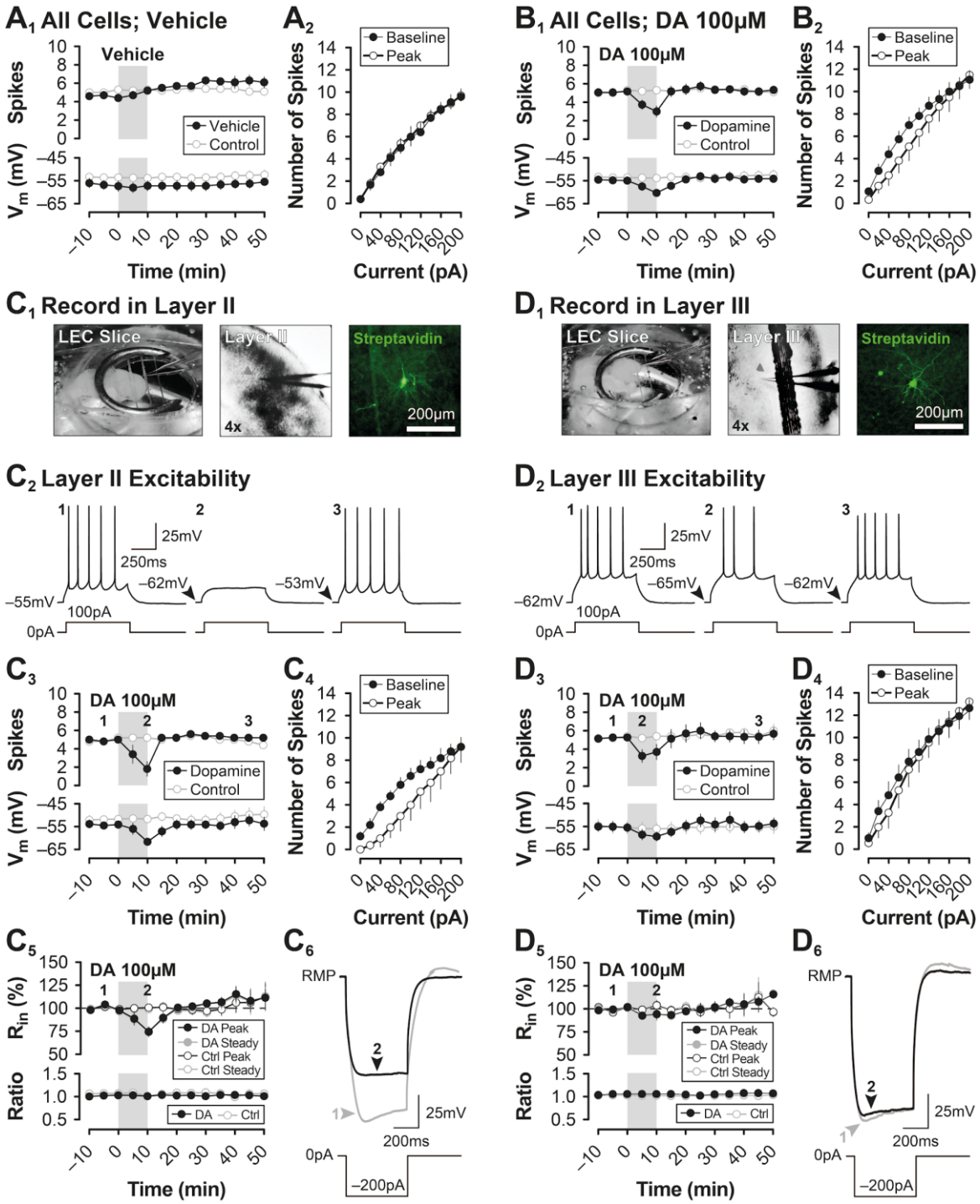

Figure 17. The intrinsic excitability of layer II and layer III projection neurons was modulated differentially by dopamine. *Bath-application of ACSF or vehicle (50 µM sodium metabisulfite) had no effect on spiking activity (**A₁**, top) or membrane potential (**A₁**, bottom) in pooled data for superficial layer projection neurons in the lateral entorhinal cortex. There was also no change in spike input-output curves before and after treatment (**A₂**). However, bath-application of 100 µM dopamine significantly reduced the number of spikes elicited by suprathreshold current injection relative to controls (**B₁**, top), and this was time-locked to a coincident and significant hyperpolarisation in the membrane potential of superficial layer neurons (**B₁**, bottom). Dopamine-mediated changes in spiking and membrane potential were transient and returned to baseline levels. There was also a slight rightward shift in the spike input-output curve following treatment with dopamine indicative of an overall reduction in excitability (**B₂**). Differential effects of dopamine on layer*

II and layer III neurons were then assessed separately. Sample images showing the recording setup for layer II neurons are shown in ***C₁*** *(wide view on the left, expanded 4x view in the middle), including an image of a biocytin-filled layer II neuron processed for streptavidin fluorescent labelling (right). Sample traces of current steps (bottom) with concurrent I-V test trace (top) in* ***C₂*** *highlight the dopamine-induced reduction in spiking before (1), immediately after treatment (2) and at the end of washout (3) in a representative layer II neuron. Numbered traces in* ***C₂*** *correspond to the time points indicated by the numbers in* ***C₃****. Overall, bath application of dopamine caused a significant, but transient, attenuation in spiking (****C₃*** *top), as well as a temporary hyperpolarisation in the membrane potential of layer II neurons (****C₃****, bottom). The peak (time-point 2) input-output curve for layer II neurons was also shifted prominently to the right highlighting the reduced excitability across a wide range of injection currents (****C₄****, open circles). Dopamine also reduced both the peak and steady-state input resistance relative to controls (****C₅****, top), but there was no effect on the rectification ratio (****C₅****, bottom). Sample current injection traces for a layer II neuron highlighting the change in membrane resistance in response to injection of a –200 pA hyperpolarising current step (****C₆****, bottom) before (grey) and after (black) dopamine are shown in* ***C₆****, top. Numbers in* ***C₆*** *correspond to latencies indicated by the numbers in* ***C₅****. Dopamine had less of an effect on layer III neurons. Conventions in* ***D₁*** *and* ***D₂*** *are the same as in* ***C₁*** *and* ***C₂*** *but for layer III. Although dopamine caused a significant attenuation of spiking in layer III neurons relative to controls (****D₃****, top), this was not accompanied by any significant change in resting membrane potential (****D₃****, bottom), spike input-output curves (****D₄****), or any measure of input resistance (****D₅*** *and* ***D₆****).*

DISCUSSION

A number of complementary techniques have been used here to demonstrate that dopaminergic inputs to the lateral entorhinal cortex have differential effects on the excitability of superficial layer projection neurons. Indeed, regardless of the recording technique used, dopamine had a suppressive effect on the intrinsic excitability of principal neurons in the lateral entorhinal cortex, and both the magnitude *and* the selectivity of this effect depended, in part, on the timing and strength of the dopamine signal itself. This is the first report to show that dopamine affects the excitability of layer II and layer III projection neurons in different ways. Specifically, principal neurons in layer II responded strongly to slow and prolonged elevations in extracellular levels of dopamine (see **Figure 17C**) whereas layer III neurons were extremely sensitive to transient and focal bursts of dopamine applied directly to the soma (see **Figure 16D**). Although projection neurons stopped spiking in response to dopamine regardless of their location in the superficial layers, the mechanisms underlying the suppression appear to be different in layer II and layer III neurons. The results of perforated patch clamp experiments suggest that a dopamine-induced change in membrane resistance (both peak and steady-state measures) resulted in a hyperpolarisation of the membrane potential to reduce spiking in layer II neurons (**Figure 17C**). This is consistent with findings from several other reports showing a similar mechanism underlying a dopamine-mediated suppression of spikes in layer II fan neurons (Pralong and Jones, 1993; Caruana and Chapman, 2008). Although layer III projection neurons reduced their firing in a similar manner (but to a lesser degree), there was no coincident change in input resistance or membrane potential observed (see **Figure 17D**). This suggests that dopamine may have a direct effect on currents involved in the generation and maintenance of spiking activity in LIII cells, such as voltage-gated sodium channels that control action potential initiation. This is the first time such an effect on excitability has been observed in layer III neurons in the lateral entorhinal cortex in response to dopamine. Taken together, these findings support the hypothesis that dopamine acts as a key signalling entity to direct the propagation of sensory information to different targets in the hippocampus by altering the firing patterns of specific populations of projection neurons in the superficial layers of the lateral entorhinal cortex. Moreover, factors related to the precise timing and duration of the dopamine signal itself may play a permissive role in determining which sub-populations of projection neurons are active at any given moment in time.

Distribution of Tyrosine Hydroxylase-Positive Fibres

Dopaminergic projections originating from the A10 cell field of the ventral tegmental area have been shown to innervate the entire laminar extent of both the medial and lateral divisions of the entorhinal cortex (Lindvall *et al*., 1974; Swanson, 1982; for review see Oades and Halliday, 1987). Indeed, the results of fluorescent immunolabeling experiments in the current study showed that tyrosine hydroxylase-positive fibres are present across all cell layers in the lateral entorhinal cortex and that there is a specific pattern in the density of innervation to each cortical layer. Specifically, fluorescent labelling was strongest in layers I, V and VI and weakest in layer II, whereas layer III showed only moderate staining for tyrosine hydroxylase (see **Figure 14B**). These findings are consistent with previous immunolabeling studies in primates (Akil and Lewis, 1993), humans (Akil and Lewis 1994) and rodents (Mingote *et al*., 2015) showing a similar pattern in the distribution of dopaminergic fibres across each layer in the entorhinal cortex. In addition, the dopaminergic fibres are located in close opposition to both the dendrites and somata of principal neurons (see **Figure 14C & 14D**), similar to previous anatomical reports, highlighting how dopaminergic axons encircle principal cell 'islands' in the most rostral portions of the lateral division (Fuxe *et al.*, 1974; Hökfelt *et al.*, 1974; Lindvall *et al.*, 1974; Collier and Routtenberg, 1978). As such, dopaminergic

fibres are positioned optimally to modulate both the input (at the dendrites) and the output (at the somata) of projection neurons in the lateral entorhinal cortex. However, tyrosine hydroxylase is the rate-limiting step required for the synthesis of *all catecholamines*, including dopamine, so it is entirely possible that the immunolabeling observed here reflects modulatory innervation by noradrenaline and not dopamine. Indeed, noradrenaline has been shown to modulate synaptic function in the superficial layers of the entorhinal cortex (see Pralong and Magistretti, 1994). However, tyrosine hydroxylase immunoreactivity is widely considered to be both a valid and reliable marker for dopaminergic neurons (Gaspar *et al.*, 1985; Lewis *et al.*, 1988; Akil and Lewis, 1994; for review see Björklund and Dunnett, 2007), and it is the gold-standard used most often for mapping the spread and distribution of dopamine-positive terminals throughout the brain. As such, it is likely that the labelling observed in the current study reflects the *actual* distribution of dopaminergic fibres in the lateral entorhinal cortex. But future experimental work should incorporate double labelling for both tyrosine hydroxylase and dopamine-β-hydroxylase (a marker for noradrenaline; see Berod *et al.*, 1982) to determine the extent that dopaminergic and noradrenergic terminals are co-expressed.

Dopaminergic Modulation of Neuronal Excitability

A high concentration of dopamine (100 µM) suppressed the activity of all neurons in the superficial layers of the lateral entorhinal cortex (**Figure 17B**), and this effect is consistent with similar studies in which dopamine was used to inhibit synaptic function (Pralong and Jones, 1993; Caruana *et al*., 2006). Arguably, the effects shown here are considerably more complex since each layer responds differently to dopamine. Layer II neurons show both a strong and rapid response to the suppressive effects of dopamine when it is bath-applied (**Figure 17C**). However, when the same concentration of dopamine is applied directly to the soma, layer II neurons do not respond nearly as intensely (or at all; **Figure 16C**). This is opposite to layer III neurons which respond rapidly and consistently to a transient puff of dopamine (**Figure 16D**). As such, these differences imply important functional and anatomical differences between layer II and layer III neuronal responses to dopamine.

It is well documented that there are five main subtypes of dopamine receptors (D_1 through to D_5) that are G-protein coupled receptors acting on key downstream regulators to affect neuronal function. D_1 and D_2 dopamine receptors are found throughout the cerebral cortex, but they are most abundant in dopamine-rich areas of the brain, including the prefrontal cortex, ventral tegmental area and entorhinal cortex (Savasta, Dubois and Scatton, 1986; Köhler, Ericson and Radesäter, 1991; Weiner *et al.*, 1991; Meador-Woodruff *et al.*, 1992). However, dopamine receptors are not distributed uniformly across cortical layers, with D_1 and D_2 receptors concentrated selectively in layers II and III in both the prefrontal and entorhinal cortices (Köhler, Ericson and Radesäter, 1991; Weiner *et al*., 1991; Stenkamp, Heinemann and Schmitz, 1998). Pharmacological characterisation of the suppressive effects of dopamine on basal synaptic function in the entorhinal cortex suggests that the depression caused by high concentrations of dopamine is mediated primarily by D_2-like dopamine receptors (Pralong and Jones, 1993; Glovaci, Caruana and Chapman, 2014; Glovaci and Chapman, 2019; for review see Seamans and Yang, 2004). Indeed, D_2-like receptors possess a large cytoplasmic loop and short carboxyl tail and are bound to $G_{i/o}$-proteins and have a higher binding affinity for dopamine relative to D_1-like receptors (for review see Seamans and Yang, 2004; Subramaniyan and Dani, 2015). Given the high affinity of D_2 receptors for dopamine and the apparent sensitivity of layer III neurons to transient and focal puffs of dopamine to the soma, it is highly likely that the suppression of spiking observed in layer III projection neurons is mediated primarily by D_2-like dopamine receptors. This is supported further in the literature by receptor expression studies showing how D_2 receptors are expressed

more prominently in layer III than they are in layer II of the entorhinal cortex (Weiner *et al.*, 1991; Stenkamp, Heinemann and Schmitz, 1998).

D_1-like dopamine receptors are also highly expressed in the lateral entorhinal cortex (Boyson, McGonigle and Molinoff, 1986; Savasta, Dubois and Scatton, 1986; Richfield, Penney and Young, 1989; Weiner *et al.*, 1991; Meador-Woodruff *et al.*, 1992), specifically in layer II (Köhler, Ericson and Radesäter, 1991). Although D_1-like receptors have been linked to a dopamine-mediated enhancement in synaptic function in the lateral entorhinal cortex (Caruana *et al*., 2006; Caruana *et al*., 2004; Glovaci *et al*., 2014; Glovaci and Chapman, 2019), they have also been shown to potentiate the suppressive effects of D_2 receptors on neuronal function (for review see Seeman and Van Tol, 1994). Indeed, low concentrations of dopamine (between 1 and 10 µM) enhance synaptic transmission via a D_1 receptor-dependent mechanism, whereas higher concentrations (50 to 100 µM) inhibit synaptic function (Caruana *et al*., 2006; Caruana and Chapman 2008) and block synaptic plasticity (Kourrich *et al.*, 2008), and this is thought to be mediated by D_2 receptors. This biphasic effect of dopamine on synaptic function is consistent with the proposed inverted 'U' shape response of dopamine in the prefrontal cortex (for review see Arnsten, 1998; Goldman-Rakic, Muly and Williams, 2000). Also, D_1 receptors, when overstimulated by high concentrations of dopamine, have been shown to enhance GABAergic transmission, and this may lead to a net suppression of pyramidal cell activity via feedforward inhibition (for review see Goldman-Rakic, Muly and Williams, 2000). As such, it is possible that some of the suppressive effects observed here may be due to overstimulation of D_1 receptors leading to a reduction in the intrinsic excitability of projection neurons in the lateral entorhinal cortex via multiple indirect mechanisms.

Dopamine is released in the brain in two important ways: tonically or phasically. There is a constant low-level background dopaminergic signal (tonic release) that helps to 'prime' dopamine receptor activity in a homeostatic way in order to maintain responsiveness to behaviourally relevant and reward-related dopamine signals (phasic release; Grace, 1991; Uehara *et al.*, 2003). The large bolus of dopamine released in response to unexpected rewards during phasic signalling is thought to activate postsynaptic dopamine receptors, including D_2-like receptors to modulate neuronal activity (Grace, 1991). Phasic dopamine is rapidly removed from extracellular space by low-affinity/high-capacity reuptake transporters before a homeostatic response ensues. As noted, tonic release of dopamine is constant with the intent to maintain a sustained background level of dopamine in various cortical and subcortical structures. Dopamine was bath-applied during a number of experiments conducted in this study, and it can be argued that this method approximates the slow tonic mode of dopamine release that occurs naturally in the brain. The addition of dopamine directly to the bathing medium had a much larger effect on projection neurons in layer II of the lateral entorhinal cortex relative to neurons in layer III (**Figure 17**). Interestingly, the dominant dopamine receptor subtype expressed in layer II is the D_1 receptor, and antagonists for D_1 receptors, such as SCH-23390, have been shown to attenuate the inhibitory actions of dopamine on synaptic transmission in the superficial layers of the medial entorhinal cortex (Pralong and Jones, 1993). These findings suggest that sustained elevations in dopaminergic tone selectively suppress activity of layer II neurons, and this may be a homeostatic mechanism that allows projection neurons in layer III to respond more preferentially to phasic dopaminergic signals from the ventral tegmental area. Indeed, layer III neurons are much more sensitive to rapid and transient puffs of dopamine than they are to prolonged and slow elevations in extracellular dopaminergic tone (**Figure 16** versus **Figure 17**). These data also complement earlier work showing that overstimulation of D_1 receptors enhances the hyperpolarising effects of D_2 receptors (for review see Arnsten, 1998; Goldman-Rakic, Muly and Williams, 2000). In addition, previous studies have shown that D_2 receptors are almost exclusively located on layer III neurons in the entorhinal cortex (Köhler, Ericson and Radesäter, 1991; Meador-Woodruff *et al*., 1992). As such, D_2 receptors

may play an important role in mediating layer III neuronal responses to short phasic bursts of dopamine.

Dopamine, Disease and the Entorhinal Cortex

It has been proposed by Otmakhova and Lisman (1999), among others, that layers II and III of the lateral entorhinal cortex play a key role in mediating the salience of sensory cues during the formation of new memories. The process is thought to start with layer III temporoammonic projections to Ammon's horn. These projections underlie the encoding of predictions by comparing pre-existing long-term memories with new incoming sensory signals entering the system. These predictions are also compared with signals arriving via the classic trisynaptic pathway. The perforant and temporoammonic input signals converge in area CA1. If the predicted information matches the new sensory information, then the new experience is not salient enough to warrant the formation of a new memory. However, if the predicted experience is mismatched with the previous memory, then the new information is encoded as a new and novel experience. This reliance on parallel -- yet complimentary -- streams of sensory information could explain why excessive dopaminergic tone isolates CA1 from specific sensory cues and limits propagation of signals from the lateral entorhinal cortex leading to a chronic state of signal mismatch. Indeed, this is a common effect seen in patients suffering from schizophrenia (Otmakhova and Lisman, 1999).

Along with schizophrenia, the lateral entorhinal cortex is thought to play a prominent role in other brain diseases, including chronic stress, major depressive disorder and Alzheimer's dementia. Indeed, Alzheimer's disease pathology usually begins in the entorhinal cortex and then spreads laterally throughout the rest of the cortex (Schultz *et al.*, 2018; Yoo *et al.*, 2018; for review see Fu, Hardy and Duff, 2018). It has been reported that deficits in olfactory processing are among some of the first symptoms observed during the early stages of the disease, as well being a consistent impairment observed in schizophrenic individuals (Yoo *et al*., 2018). Neurofibrillary tangles, a large bundle of protein that eventually becomes toxic to neurons, was found to be the main contributing factor leading to deficits in olfactory function. Tangles have been shown to be especially prevalent in the entorhinal cortex, as well as in area CA1 of the hippocampus, during the initial stages of the disease (Yoo *et al*., 2018). It is notable that layer III projection neurons in the lateral entorhinal cortex neurons innervate area CA1 directly via the temporoammonic path, and neurons in layer III are extremely sensitive to dopamine. In the current study, layer III neurons have been shown to respond strongly to phasic release of dopamine, suggesting that temporoammonic inputs to area CA1 are modulated exclusively by dopamine. In a review by Stranahan and Mattson (2010) it was suggested that activity of layer II entorhinal cortex neurons, which form perforant path inputs to the dentate gyrus and area CA3, are impaired in aging and Alzheimer's disease, but the selective vulnerability is unknown. It therefore becomes immensely important to investigate the dopaminergic modulation of superficial layers of the lateral entorhinal cortex.

Both chronic stress and depression are thought to involve neuronal pathology leading to cell death. Sunanda, Meti and Raju (1997) proposed that the atrophy of CA3 neurons linked to restraint-induced stress resulted from a dysfunction originating in the entorhinal cortex. Indeed, they observed that glutamatergic denervation of the entorhinal cortex prior to stress protected CA3 dendrites and attenuated the neuronal atrophy (Sunanda, Meti and Raju, 1997). It was hypothesised that hyperexcitation in entorhinal efferent projections to the hippocampus was leading to elevations in extracellular glutamate triggering excitotoxic neuronal death in area CA3, specifically. This is the same mechanism that is thought to play a key role in the aetiology of

Alzheimer's dementia (Sunanda, Meti and Raju, 1997). Area CA3 receives input via perforant path projections originating from layer II neurons in the entorhinal cortex, and it is these neurons specifically that are thought to play a role in the homeostatic regulation of dopamine receptor function induced by tonic changes in extracellular dopamine levels (Köhler, Ericson and Radesäter, 1991; Pralong and Jones, 1993; Stenkamp, Heinemann and Schmitz, 1998; Mayne *et al.*, 2013). As such, an increase in dopamine, similar to the addition of 100 µM dopamine to the perfusate during slice recording experiments, would lead to a widespread suppression of excitability in entorhinal cortex projection neurons and prevent excitotoxicity from occurring in target regions, including area CA3 (for review see Arnsten, 1998; Goldman-Rakic, Muly and Williams, 2000). This protective mechanism may fail in individuals suffering from chronic stress resulting in severe atrophy of CA3 neurons and other regions, including the amygdala.

Chronic stress-induced damage to the entorhinal cortex has been shown to cause profound changes in dopaminergic signalling within the lateral amygdala (Uehara *et al*., 2003). Specifically, changes in entorhinal communication with the amygdala induced by periods of chronic stress leads to elevations in extracellular dopamine levels in the lateral amygdala. It was also found that lesioning the entorhinal cortex not only prevents formation of new spatial and non-spatial memories (Sunanda, Meti and Raju, 1997), but also increases phasic dopaminergic transmission in subcortical brain regions, including the lateral amygdala. In addition, Avital *et al.* (2006) exposed juvenile rats to stress and tracked levels of dehydroepiandrosterone (DHEA), an endogenous hormone secreted by the adrenal gland and produced in the central nervous system as a neurosteroid acting as a negative modulator of inhibitory receptors, in the entorhinal cortex. They found DHEAs in a healthy, stress-free adult rat exhibited memory-enhancing, antidepressant properties, but in adult rats that suffered a highly stressful period as a juvenile were less active and more anxious with significantly more DHEA molecules in the entorhinal cortex than were there during the stressful period. This change in DHEA concentration and subsequent change in behaviour may aid in the understanding of stress-related disorders like depression (Avital *et al*., 2006). It is also important to underscore how changes in the entorhinal cortex function mediated by local changes in neuromodulation can have dramatic effects on any number of downstream mechanisms leading to profound changes in the functioning of these target brain regions.

Summary and Conclusions

The formation of new declarative memories is an extremely complex process involving widespread network interactions, a multitude of sensory cues, and a variety of neuromodulatory signals. Dysfunction in any small part of this interconnected system can have devastating effects on the ability to acquire new information and to remember it over time. The entorhinal cortex plays an important part in this process by functioning as a critical node between multiple sensory systems and the hippocampal formation. More specifically, the entorhinal cortex encodes key signals related to space, direction and velocity, as well as signals concerning odour and object identity. These multiple streams of sensory information are relayed to different targets in the hippocampus where they are integrated with contextual and temporal cues, and then compared to previous experience. As such, communication and information flow between the entorhinal cortex and hippocampus is essential, and dysfunctions in this process can have dramatic effects on immediate behavioural output and long-term information processing, including the formation of new declarative memories. The results of this thesis provide exciting new evidence showcasing how dopamine contributes to the underlying physiology of these important cognitive functions by affecting the propagation of sensory signals to the hippocampus via changes in projection neuron output.

REFERENCES

Akil, M. and Lewis, D. A. (1993) 'The Dopaminergic Innervation of Monkey Entorhinal Cortex', Cerebral Cortex, 3(6), pp. 533–550. doi: 10.1093/cercor/3.6.533.

Akil, M. and Lewis, D. A. (1994) 'The distribution of tyrosine hydroxylase-immunoreactive fibers in the human entorhinal cortex', Neuroscience, 60(4), pp. 857–874. doi: 10.1016/0306-4522(94)90268-2.

Arnsten, A. F. T. (1998) 'Catecholamine modulation of prefrontal cortical cognitive function', Trends in Cognitive Sciences, 2(11), pp. 436–447. doi: 10.1016/S1364-6613(98)01240-6.

Avital, A., Ram, E., Maayan, R., Weizman, A. and Richter-Levin, G. (2006) 'Effects of early-life stress on behavior and neurosteroid levels in the rat hypothalamus and entorhinal cortex', Brain Research Bulletin, 68(6), pp. 419–424. doi: 10.1016/j.brainresbull.2005.09.015.

Batallán-Burrowes, A. A. and Chapman, C. A. (2018) 'Dopamine suppresses persistent firing in layer III lateral entorhinal cortex neurons', Neuroscience Letters. Elsevier, 674(March), pp. 70–74. doi: 10.1016/j.neulet.2018.03.012.

Beaulieu, J.-M., Espinoza, S. and Gainetdinov, R. R. (2015) 'Dopamine receptors - IUPHAR Review 13', British Journal of Pharmacology. John Wiley and Sons Inc., 172(1), pp. 1–23. doi: 10.1111/bph.12906.

Berod, A., Hartman, B. K., Keller, A., Joh, T. H. and Pujol, J. F. (1982) 'A new double labeling technique using tyrosine hydroxylase and dopamine-β-hydroxylase immunohistochemistry: Evidence for dopaminergic cells lying in the pons of the beef brain', Brain Research. doi: 10.1016/0006-8993(82)90219-0.

Björklund, A. and Dunnett, S. B. (2007) 'Dopamine neuron systems in the brain: an update', Trends in Neurosciences, 30(5), pp. 194–202. doi: 10.1016/j.tins.2007.03.006.

Blackstad, T. W. (1958) 'On the termination of some afferents to the hippocampus and fascia dentata; an experimental study in the rat.', Cells Tissues Organs, 35(3), pp. 202–214. doi: 10.1159/000141409.

Boyson, S. J., McGonigle, P. and Molinoff, P. B. (1986) 'Quantitative autoradiographic localization of the D1 and D2 subtypes of dopamine receptors in rat brain', Journal of Neuroscience, 6(11), pp. 3177–3188. doi: 10.1523/jneurosci.06-11-03177.1986.

Burwell, R. D. (2006) 'The Parahippocampal Region: Corticocortical Connectivity', Annals of the New York Academy of Sciences, 911(1), pp. 25–42. doi: 10.1111/j.1749-6632.2000.tb06717.x.

Canto, C. B. and Witter, M. P. (2012) 'Cellular properties of principal neurons in the rat entorhinal cortex. I. The lateral entorhinal cortex', Hippocampus, 22(6), pp. 1256–1276. doi: 10.1002/hipo.20997.

Canto, C. B., Wouterlood, F. G. and Witter, M. P. (2008) 'What Does the Anatomical Organization of the Entorhinal Cortex Tell Us?', Neural Plasticity, 2008, pp. 1–18. doi: 10.1155/2008/381243.

Carboni, A. A. and Lavelle, W. G. (2000) 'Ultrastructural Characterizations of Olfactory Pathway Neurons in Layer II of the Entorhinal Cortex in Monkey', Acta Oto-Laryngologica, 120(3), pp. 424–431. doi: 10.1080/000164800750000685.

Caruana, D. A., Sorge, R. E., Stewart, J. and Chapman, C. A. (2006) 'Dopamine Has Bidirectional Effects on Synaptic Responses to Cortical Inputs in Layer II of the Lateral Entorhinal Cortex', Journal of Neurophysiology, 96(6), pp. 3006–3015. doi: 10.1152/jn.00572.2006.

Caruana, D. A. and Chapman, C. A. (2008) 'Dopaminergic Suppression of Synaptic Transmission in the Lateral Entorhinal Cortex', Neural Plasticity, 2008, pp. 1–14. doi: 10.1155/2008/203514.

Caruana, D. A. and Dudek, S. M. (2020) 'Adenosine A1 Receptor-Mediated Synaptic Depression in the Developing Hippocampal Area CA2', Frontiers in Synaptic Neuroscience, 12(May), pp. 1–17. doi: 10.3389/fnsyn.2020.00021.

Caruana, D. A., Warburton, E. C. and Bashir, Z. I. (2011) 'Induction of Activity-Dependent LTD Requires Muscarinic Receptor Activation in Medial Prefrontal Cortex', Journal of Neuroscience, 31(50), pp. 18464–18478. doi: 10.1523/JNEUROSCI.4719-11.2011.

Chapman, C. A. and Lacaille, J.-C. (1999) 'Intrinsic Theta-Frequency Membrane Potential Oscillations in Hippocampal CA1 Interneurons of Stratum Lacunosum-Moleculare', Journal of Neurophysiology, 81(3), pp. 1296–1307. doi: 10.1152/jn.1999.81.3.1296.

Collier, T. J. and Routtenberg, A. (1978) 'Entorhinal cortex electrical stimulation disrupts retention performance when applied after, but not during, learning', Brain Research. doi: 10.1016/0006-8993(78)90274-3.

Davie, J. T., Kole, M. H. P., Letzkus, J. J., Rancz, E. A., Spruston, N., Stuart, G. J. and Häusser, M. (2006) 'Dendritic patch-clamp recording', Nature Protocols, 1(3), pp. 1235–1247. doi: 10.1038/nprot.2006.164.

Deshmukh, S. S. and Knierim, J. J. (2011) 'Representation of Non-Spatial and Spatial Information in the Lateral Entorhinal Cortex', Frontiers in Behavioral Neuroscience, 5. doi: 10.3389/fnbeh.2011.00069.

Dickson, C. T., Magistretti, J., Shalinsky, M. H., Fransén, E., Hasselmo, M. E. and Alonso, A. (2000) 'Properties and Role of I h in the Pacing of Subthreshold Oscillations in Entorhinal Cortex Layer II Neurons', Journal of Neurophysiology, 83(5), pp. 2562–2579. doi: 10.1152/jn.2000.83.5.2562.

Egorov, A. V., Hamam, B. N., Fransén, E., Hasselmo, M. E. and Alonso, A. A. (2002) 'Graded persistent activity in entorhinal cortex neurons', Nature, 420(6912), pp. 173–178. doi: 10.1038/nature01171.

Fallon, J. H., Koziell, D. A. and Moore, R. Y. (1978) 'Catecholamine innervation of the basal forebrain II. Amygdala, suprarhinal cortex and entorhinal cortex', The Journal of Comparative Neurology, 180(3), pp. 509–531. doi: 10.1002/cne.901800308.

Fu, H., Hardy, J. and Duff, K. E. (2018) 'Selective vulnerability in neurodegenerative diseases', Nature Neuroscience. Nature Publishing Group, 21(10), pp. 1350–1358. doi: 10.1038/s41593-018-0221-2.

Fukawa, A., Aizawa, T., Yamakawa, H. and Eguchi Yairi, I. (2020) 'Identifying Core Regions for Path Integration on Medial Entorhinal Cortex of Hippocampal Formation', Brain Sciences, 10(1), p. 28. doi: 10.3390/brainsci10010028.

Fuxe, K. (1965) 'Evidence for the existence of monoamine neurons in the central nervous system',

Zeitschrift for Zellforschung und Mikroskopische Anatomie, 65(4), pp. 573–596. doi: 10.1007/BF00337069.

Fuxe, K., Hökfelt, T., Johansson, O., Jonsson, G., Lidbrink, P. and Ljundahl, Å. (1974) 'The origin of the dopamine nerve terminals in limbic and frontal cortex. Evidence for meso-cortico dopamine neurons', Brain Research. doi: 10.1016/0006-8993(74)90618-0.

Gaspar, P., Berger, B., Alvarez, C., Vigny, A. and Henry, J. P. (1985) 'Catecholaminergic innervation of the septal area in man: Immunocytochemical study using TH and DBH antibodies', Journal of Comparative Neurology. doi: 10.1002/cne.902410103.

Ghannoum, M. A. and Rice, L. B. (1999) 'Antifungal Agents: Mode of Action, Mechanisms of Resistance, and Correlation of These Mechanisms with Bacterial Resistance', Clinical Microbiology Reviews, 12(4), pp. 501–517. doi: 10.1128/CMR.12.4.501.

Giocomo, L. M. and Hasselmo, M. E. (2008) 'Time Constants of h Current in Layer II Stellate Cells Differ along the Dorsal to Ventral Axis of Medial Entorhinal Cortex', Journal of Neuroscience, 28(38), pp. 9414–9425. doi: 10.1523/JNEUROSCI.3196-08.2008.

Glovaci, I., Caruana, D. A. and Chapman, C. A. (2014) 'Dopaminergic enhancement of excitatory synaptic transmission in layer II entorhinal neurons is dependent on D1-like receptor-mediated signaling', Neuroscience, 258, pp. 74–83. doi: 10.1016/j.neuroscience.2013.10.076.

Glovaci, I. and Chapman, C. A. (2015) 'Activation of Phosphatidylinositol-Linked Dopamine Receptors Induces a Facilitation of Glutamate-Mediated Synaptic Transmission in the Lateral Entorhinal Cortex', PLOS ONE. Edited by G. Fisone, 10(7), p. e0131948. doi: 10.1371/journal.pone.0131948.

Glovaci, I. and Chapman, C. A. (2019) 'Dopamine induces release of calcium from internal stores in layer II lateral entorhinal cortex fan cells.', Cell Calcium. Elsevier, 80(November 2018), pp. 103–111. doi: 10.1016/j.ceca.2019.04.003.

Goldman-Rakic, P. (2000) 'D1 receptors in prefrontal cells and circuits', Brain Research Reviews, 31(2–3), pp. 295–301. doi: 10.1016/S0165-0173(99)00045-4.

Grace, A. A. (1991) 'Phasic versus tonic dopamine release and the modulation of dopamine system responsivity: A hypothesis for the etiology of schizophrenia', Neuroscience, 41(1), pp. 1–24. doi: 10.1016/0306-4522(91)90196-U.

Hargreaves, E. L. (2005) 'Major Dissociation Between Medial and Lateral Entorhinal Input to Dorsal Hippocampus', Science, 308(5729), pp. 1792–1794. doi: 10.1126/science.1110449.

Hasbi, A., O'Dowd, B. F. and George, S. R. (2010) 'Heteromerization of dopamine D2 receptors with dopamine D1 or D5 receptors generates intracellular calcium signaling by different mechanisms', Current Opinion in Pharmacology, 10(1), pp. 93–99. doi: 10.1016/j.coph.2009.09.011.

Hasselmo, M. E., Hay, J., Ilyn, M. and Gorchetchnikov, A. (2002) 'Neuromodulation, theta rhythm and rat spatial navigation', Neural Networks, 15(4–6), pp. 689–707. doi: 10.1016/S0893-6080(02)00057-6.

Hasselmo, M. E. (2006) 'The role of acetylcholine in learning and memory', Current Opinion in Neurobiology, 16(6), pp. 710–715. doi: 10.1016/j.conb.2006.09.002.

Heys, J. G. and Hasselmo, M. E. (2012) 'Neuromodulation of Ih in Layer II Medial Entorhinal Cortex Stellate Cells: A Voltage-Clamp Study', Journal of Neuroscience, 32(26), pp. 9066–9072. doi:

10.1523/JNEUROSCI.0868-12.2012.

Hökfelt, T., Fuxe, K., Goldstein, M. and Johansson, O. (1974) 'Immunohistochemical evidence for the existence of adrenaline neurons in the rat brain', Brain Research. doi: 10.1016/0006-8993(74)90143-7.

Ishibashi, H., Moorhouse, A. J. and Nabekura, J. (2012) 'Perforated Whole-Cell Patch-Clamp Technique: A User's Guide', in Patch Clamp Techniques, pp. 71–83. doi: 10.1007/978-4-431-53993-3_4.

Iwase, M., Kitanishi, T. and Mizuseki, K. (2020) 'Cell type, sub-region, and layer-specific speed representation in the hippocampal–entorhinal circuit', Scientific Reports, 10(1), p. 1407. doi: 10.1038/s41598-020-58194-1.

Jones, M. W. and McHugh, T. J. (2011) 'Updating hippocampal representations: CA2 joins the circuit', Trends in Neurosciences, 34(10), pp. 526–535. doi: 10.1016/j.tins.2011.07.007.

Kloosterman, F., van Haeften, T. and Lopes da Silva, F. H. (2004) 'Two reentrant pathways in the hippocampal-entorhinal system', Hippocampus, 14(8), pp. 1026–1039. doi: 10.1002/hipo.20022.

Köhler, C., Ericson, H. and Radesäter, A.-C. (1991) 'Different laminar distributions of dopamine D1 and D2 receptors in the rat hippocampal region', Neuroscience Letters, 126(2), pp. 107–109. doi: 10.1016/0304-3940(91)90530-7.

Kourrich, S., Glasgow, S. D., Caruana, D. A. and Chapman, C. A. (2008) 'Postsynaptic signals mediating induction of long-term synaptic depression in the entorhinal cortex', Neural Plasticity. Hindawi Publishing Corporation, 2008. doi: 10.1155/2008/840374.

Lewis, D. A., Foote, S. L., Goldstein, M. and Morrison, J. H. (1988) 'The dopaminergic innervation of monkey prefrontal cortex: a tyrosine hydroxylase immunohistochemical study', Brain Research. doi: 10.1016/0006-8993(88)91040-2.

Lindvall, O., Björklund, A., Moore, R. Y. and Stenevi, U. (1974) 'Mesencephalic dopamine neurons projecting to neocortex', Brain Research, 81(2), pp. 325–331. doi: 10.1016/0006-8993(74)90947-0.

Lingenhöhl, K. and Finch, D. M. (1991) 'Morphological characterization of rat entorhinal neurons in vivo: soma-dendritic structure and axonal domains', Experimental Brain Research, 84(1). doi: 10.1007/BF00231762.

Lucas, S. J. and Armstrong, D. L. (2015) 'Protein phosphatase modulation of somatostatin receptor signaling in the mouse hippocampus', Neuropharmacology. Elsevier Ltd, 99, pp. 232–241. doi: 10.1016/j.neuropharm.2015.07.004.

Mayne, E. W., Craig, M. T., McBain, C. J. and Paulsen, O. (2013) 'Dopamine suppresses persistent network activity via D 1 -like dopamine receptors in rat medial entorhinal cortex', European Journal of Neuroscience, 37(8), pp. 1242–1247. doi: 10.1111/ejn.12125.

Meador-Woodruff, J. H., Mansour, A., Grandy, D. K., Damask, S. P., Civelli, O. and Watson, S. J. (1992) 'Distribution of D5 dopamine receptor mRNA in rat brain', Neuroscience Letters, 145(2), pp. 209–212. doi: 10.1016/0304-3940(92)90024-2.

Mingote, S., Chuhma, N., Kusnoor, S. V., Field, B., Deutch, A. Y. and Rayport, S. (2015) 'Functional Connectome Analysis of Dopamine Neuron Glutamatergic Connections in Forebrain Regions', Journal of Neuroscience, 35(49), pp. 16259–16271. doi: 10.1523/JNEUROSCI.1674-15.2015.

Moser, E. I., Roudi, Y., Witter, M. P., Kentros, C., Bonhoeffer, T. and Moser, M.-B. (2014) 'Grid cells

and cortical representation', Nature Reviews Neuroscience. Nature Publishing Group, 15(7), pp. 466–481. doi: 10.1038/nrn3766.

Moser, E. I., Kropff, E. and Moser, M.-B. (2008) 'Place cells, grid cells, and the brain's spatial representation system.', Annual review of neuroscience, 31, pp. 69–89. doi: 10.1146/annurev.neuro.31.061307.090723.

Neve, K. A., Seamans, J. K. and Trantham-Davidson, H. (2004) 'Dopamine Receptor Signaling', Journal of Receptors and Signal Transduction, 24(3), pp. 165–205. doi: 10.1081/RRS-200029981.

Nilssen, E. S., Doan, T. P., Nigro, M. J., Ohara, S. and Witter, M. P. (2019) 'Neurons and networks in the entorhinal cortex: A reappraisal of the lateral and medial entorhinal subdivisions mediating parallel cortical pathways', Hippocampus, 29(12), pp. 1238–1254. doi: 10.1002/hipo.23145.

Oades, R. D. and Halliday, G. M. (1987) 'Ventral tegmental (A10) system: neurobiology. 1. Anatomy and connectivity', Brain Research Reviews, 12(2), pp. 117–165. doi: 10.1016/0165-0173(87)90011-7.

Otmakhova, N. A. and Lisman, J. E. (1999) 'Dopamine Selectively Inhibits the Direct Cortical Pathway to the CA1 Hippocampal Region', The Journal of Neuroscience, 19(4), pp. 1437–1445. doi: 10.1523/JNEUROSCI.19-04-01437.1999.

Paxinos, G. and Watson, C. (2007) The Rat Brain in Stereotaxic Coordinates Sixth Edition, Elsevier Academic Press.

Pralong, E. and Jones, R. S. G. (1993) 'Interactions of Dopamine with Glutamate- and GABA-mediated Synaptic Transmission in the Rat Entorhinal Cortex In Vitro', European Journal of Neuroscience, 5(6), pp. 760–767. doi: 10.1111/j.1460-9568.1993.tb00540.x.

Pralong, E. and Magistretti, P. J. (1994) 'Noradrenaline reduces synaptic responses in normal and tottering mouse entorhinal cortex via α2 receptors', Neuroscience Letters. doi: 10.1016/0304-3940(94)90955-5.

Ray, S. and Brecht, M. (2016) 'Structural development and dorsoventral maturation of the medial entorhinal cortex', eLife, 5(APRIL2016), pp. 1–16. doi: 10.7554/eLife.13343.

Richfield, E. K., Penney, J. B. and Young, A. B. (1989) 'Anatomical and affinity state comparisons between dopamine D1 and D2 receptors in the rat central nervous system', Neuroscience, 30(3), pp. 767–777. doi: 10.1016/0306-4522(89)90168-1.

Rosenkranz, J. A. (2006) 'Dopaminergic Regulation of Neuronal Excitability through Modulation of Ih in Layer V Entorhinal Cortex', Journal of Neuroscience, 26(12), pp. 3229–3244. doi: 10.1523/JNEUROSCI.4333-05.2006.

Sarantopoulos, C. (2007) 'Perforated Patch-Clamp Techniques', in Patch-Clamp Analysis, pp. 253–293. doi: 10.1007/978-1-59745-492-6_8.

Savasta, M., Dubois, A. and Scatton, B. (1986) 'Autoradiographic localization of D1 dopamine receptors in the rat brain with [3H]SCH 23390', Brain Research, 375(2), pp. 291–301. doi: 10.1016/0006-8993(86)90749-3.

Schultz, S. A., Gordon, B. A., Mishra, S., Su, Y., Perrin, R. J., Cairns, N. J., Morris, J. C., Ances, B. M. and Benzinger, T. L. S. (2018) 'Widespread distribution of tauopathy in preclinical Alzheimer's disease', Neurobiology of Aging, 72, pp. 177–185. doi: 10.1016/j.neurobiolaging.2018.08.022.

Seamans, J. K. and Yang, C. R. (2004) 'The principal features and mechanisms of dopamine modulation in the prefrontal cortex', Progress in Neurobiology, 74(1), pp. 1–58. doi: 10.1016/j.pneurobio.2004.05.006.

Seeman, P. and Van Tol, H. H. M. (1994) 'Dopamine receptor pharmacology', Trends in Pharmacological Sciences, 15(7), pp. 264–270. doi: 10.1016/0165-6147(94)90323-9.

Segev, A., Garcia-Oscos, F. and Kourrich, S. (2016) 'Whole-cell Patch-clamp Recordings in Brain Slices', Journal of Visualized Experiments, 2016(112), pp. 1–10. doi: 10.3791/54024.

Simons, S. B., Caruana, D. A., Zhao, M. and Dudek, S. M. (2012) 'Caffeine-induced synaptic potentiation in hippocampal CA2 neurons', Nature Neuroscience, 15(1), pp. 23–25. doi: 10.1038/nn.2962.

Solodkin, A. and Van Hoesen, G. W. (1996) 'Entorhinal cortex modules of the human brain', The Journal of Comparative Neurology, 365(4), pp. 610–627. doi: 10.1002/(SICI)1096-9861(19960219)365:4<610::AID-CNE8>3.0.CO;2-7.

Stenkamp, K., Heinemann, U. and Schmitz, D. (1998) 'Dopamine suppresses stimulus-induced field potentials in layer III of rat medial entorhinal cortex', Neuroscience Letters, 255(2), pp. 119–121. doi: 10.1016/S0304-3940(98)00721-6.

Steward, O. (1976) 'Topographic organization of the projections from the entorhinal area to the hippocampal formation of the rat', The Journal of Comparative Neurology, 167(3), pp. 285–314. doi: 10.1002/cne.901670303.

Stranahan, A. M. and Mattson, M. P. (2010) 'Selective Vulnerability of Neurons in Layer II of the Entorhinal Cortex during Aging and Alzheimer's Disease', Neural Plasticity. Hindawi Publishing Corporation, 2010, pp. 1–8. doi: 10.1155/2010/108190.

Subramaniyan, M. and Dani, J. A. (2015) 'Dopaminergic and cholinergic learning mechanisms in nicotine addiction', Annals of the New York Academy of Sciences, 1349(1), pp. 46–63. doi: 10.1111/nyas.12871.

Sunanda, Meti, B. . and Raju, T. . (1997) 'Entorhinal cortex lesioning protects hippocampal CA3 neurons from stress-induced damage', Brain Research, 770(1–2), pp. 302–306. doi: 10.1016/S0006-8993(97)00888-3.

Swanson, L. W. (1982) 'The projections of the ventral tegmental area and adjacent regions: A combined fluorescent retrograde tracer and immunofluorescence study in the rat', Brain Research Bulletin, 9(1–6), pp. 321–353. doi: 10.1016/0361-9230(82)90145-9.

Tahvildari, B. and Alonso, A. (2005) 'Morphological and electrophysiological properties of lateral entorhinal cortex layers II and III principal neurons', The Journal of Comparative Neurology, 491(2), pp. 123–140. doi: 10.1002/cne.20706.

Uehara, T., Sumiyoshi, T., Itoh, H. and Kurachi, M. (2003) 'Modulation of stress-induced dopamine release by excitotoxic damage of the entorhinal cortex in the rat', Brain Research, 989(1), pp. 112–116. doi: 10.1016/S0006-8993(03)03363-8.

Vandrey, B., Garden, D. L. F., Ambrozova, V., McClure, C., Nolan, M. F. and Ainge, J. A. (2020) 'Fan Cells in Layer 2 of the Lateral Entorhinal Cortex Are Critical for Episodic-like Memory', Current Biology, 30(1), pp. 169-175.e5. doi: 10.1016/j.cub.2019.11.027.

Weiner, D. M., Levey, A. I., Sunahara, R. K., Niznik, H. B., O'Dowd, B. F., Seeman, P. and Brann, M. R. (1991) 'D1 and D2 dopamine receptor mRNA in rat brain.', Proceedings of the National Academy of Sciences, 88(5), pp. 1859–1863. doi: 10.1073/pnas.88.5.1859.

Witter, M. P., Doan, T. P., Jacobsen, B., Nilssen, E. S. and Ohara, S. (2017) 'Architecture of the Entorhinal Cortex A Review of Entorhinal Anatomy in Rodents with Some Comparative Notes', Frontiers in Systems Neuroscience, 11(June), pp. 1–12. doi: 10.3389/fnsys.2017.00046.

Wyss, M. J. (1981) 'An autoradiographic study of the efferent connections of the entorhinal cortex in the rat', The Journal of Comparative Neurology, 199(4), pp. 495–512. doi: 10.1002/cne.901990405.

Yang, C., Seamans, J. and Gorelova, N. (1996) 'Electrophysiological and morphological properties of layers V-VI principal pyramidal cells in rat prefrontal cortex in vitro', The Journal of Neuroscience, 16(5), pp. 1904–1921. doi: 10.1523/JNEUROSCI.16-05-01904.1996.

Yoo, H. S., Jeon, S., Chung, S. J., Yun, M., Lee, P. H., Sohn, Y. H., Evans, A. C. and Ye, B. S. (2018) 'Olfactory dysfunction in Alzheimer's disease- and Lewy body-related cognitive impairment', Alzheimer's & Dementia. Elsevier Inc., 14(10), pp. 1243–1252. doi: 10.1016/j.jalz.2018.05.010.

Appendices

Appendix A

One-way ANOVA

ANOVA table	SS	DF	MS	F (DFn, DFd)	P value
Treatment (between columns)	1645	3	548.5	F (3, 16) = 33.06	P<0.0001
Residual (within columns)	265.4	16	16.59		
Total	1911	19			

Bonferroni's multiple comparisons test

Bonferroni's multiple comparisons test	Mean Diff.	95.00% CI of diff.	Significant?	Summary	Adjusted P Value
LI vs. LII	19.58	11.83 to 27.32	Yes	****	<0.0001
LI vs. LIII	10.34	2.595 to 18.09	Yes	**	0.0060
LI vs. LV-VI	-3.556	-11.31 to 4.193	No	ns	>0.9999
LII vs. LIII	-9.231	-16.98 to -1.482	Yes	*	0.0149
LII vs. LV-VI	-23.13	-30.88 to -15.38	Yes	****	<0.0001
LIII vs. LV-VI	-13.90	-21.65 to -6.151	Yes	***	0.0004

Descriptive Statistics

	LI	LII	LIII	LV-VI
Number of values	5	5	5	5
Minimum	25.08	9.421	18.78	31.34
25% Percentile	26.90	9.726	18.97	31.43
Median	30.57	10.79	21.29	33.13
75% Percentile	36.79	14.92	23.50	39.88
Maximum	38.92	15.01	24.66	43.17
Mean	31.59	12.02	21.25	35.15
Std. Deviation	5.358	2.694	2.412	4.957
Std. Error of Mean	2.396	1.205	1.079	2.217
Lower 95% CI	24.94	8.670	18.25	28.99
Upper 95% CI	38.24	15.36	24.24	41.30

One-way ANOVA, Bonferroni's multiple comparisons test and descriptive statistics on data displayed in Figure 14.

Appendix B

Mixed effects analysis

Fixed effects (type III)	P value	P value summary	Statistically significant (P < 0.05)?	F (DFn, DFd)
Time	0.0532	ns	No	F (1.786, 8.036) = 4.440
Group	0.0584	ns	No	F (2, 12) = 3.634
Time x Group	0.5450	ns	No	F (4, 9) = 0.8179

Bonferroni's multiple comparisons

Bonferroni's multiple comparisons test	Mean Diff.	95.00% CI of diff.	Significant?	Summary	Adjusted P Value
ACSF					
Baseline vs. Post-Drug	49.17	-51.92 to 150.3	No	ns	0.3009
Baseline vs. Washout	30.39	-414.1 to 474.9	No	ns	>0.9999
Post-Drug vs. Washout	-18.78	-414.8 to 377.2	No	ns	>0.9999
Vehicle					
Baseline vs. Post-Drug	96.03	-28.12 to 220.2	No	ns	0.1131
Baseline vs. Washout	82.38	-34.17 to 198.9	No	ns	0.1797
Post-Drug vs. Washout	-13.64	-80.94 to 53.65	No	ns	>0.9999
DA 100μM					
Baseline vs. Post-Drug	100.0	-564.1 to 764.1	No	ns	0.3289
Baseline vs. Washout	64.49	-278.8 to 407.7	No	ns	0.6497
Post-Drug vs. Washout	-35.51	-1115 to 1044	No	ns	>0.9999

Mixed effects analysis tabular results and Bonferroni's multiple comparisons test on whole-cell patch during micropipette dialysis data displayed in Figure 15 $A_{1\text{-}4}$.

Mixed effects analysis

Fixed effects (type III)	P value	P value summary	Statistically significant (P < 0.05)?	F (DFn, DFd)
Time	0.5847	ns	No	F (1.388, 35.40) = 0.4239
Group	0.0608	ns	No	F (2, 51) = 2.959
Time x Group	0.6136	ns	No	F (4, 51) = 0.6732

Bonferroni's multiple comparisons test

Bonferroni's multiple comparisons test	Mean Diff.	95.00% CI of diff.	Significant?	Summary	Adjusted P Value
ACSF					
Baseline vs. Post-Drug	27.85	-134.1 to 189.8	No	ns	>0.9999
Baseline vs. Washout	14.77	-158.1 to 187.6	No	ns	>0.9999
Post-Drug vs. Washout	-13.08	-170.0 to 143.9	No	ns	>0.9999
Vehicle					
Baseline vs. Post-Drug	65.97	-16.96 to 148.9	No	ns	0.1349
Baseline vs. Washout	47.64	-39.26 to 134.5	No	ns	0.4508
Post-Drug vs. Washout	-18.33	-82.61 to 45.94	No	ns	>0.9999
DA 100µM					
Baseline vs. Post-Drug	100.0	-27.40 to 227.4	No	ns	0.1175
Baseline vs. Washout	-5.025	-183.3 to 173.3	No	ns	>0.9999
Post-Drug vs. Washout	-105.0	-279.1 to 69.00	No	ns	0.2583

Mixed effects analysis tabular results and Bonferroni's multiple comparisons test on whole-cell patch after micropipette dialysis data displayed in Figure 15 $B_{1\text{-}4}$.

Appendix C

Paired t-test – LII ACSF

Paired t test	
P value	0.5046
P value summary	ns
Significantly different (P < 0.05)?	No
One- or two-tailed P value?	Two-tailed
t, df	t=0.7185, df=5
Number of pairs	6

Descriptive statistics -LII ACSF

Paired t test Descriptive statistics	Pre-Puff	Post-Puff	Post-Puff - Pre-Puff
Number of values	6	6	6
Minimum	1.667	0.000	-4.000
25% Percentile	3.167	0.7500	-1.500
Median	4.333	5.500	0.6667
75% Percentile	7.750	13.75	3.833
Maximum	14.00	16.00	8.333
Mean	5.611	6.833	1.222
Std. Deviation	4.317	6.616	4.167
Std. Error of Mean	1.763	2.701	1.701
Lower 95% CI	1.080	-0.1094	-3.151
Upper 95% CI	10.14	13.78	5.595

Paired t-test and descriptive statistics on whole cell patch puff data of LII ACSF cells displayed in Figure 16 $B_{2,4}$

Paired t-test – LIII ACSF

Paired t test	
P value	0.0623
P value summary	ns
Significantly different (P < 0.05)?	No
One- or two-tailed P value?	Two-tailed
t, df	t=2.565, df=4
Number of pairs	5

Descriptive statistics – LIII ACSF

Paired t test Descriptive statistics	Pre-Puff	Post-Puff	Post-Puff - Pre-Puff
Number of values	5	5	5
Minimum	1.333	0.000	-4.000
25% Percentile	1.500	0.000	-2.833
Median	4.000	1.000	-1.333
75% Percentile	6.667	5.500	-0.6667
Maximum	8.333	7.000	0.000
Mean	4.067	2.400	-1.667
Std. Deviation	2.842	3.050	1.453
Std. Error of Mean	1.271	1.364	0.6498
Lower 95% CI	0.5377	-1.387	-3.471
Upper 95% CI	7.596	6.187	0.1374

Paired t-test and descriptive statistics on whole cell patch puff data of LIII ACSF cells displayed in Figure 16 $B_{3,4}$

Paired t-test – combined ACSF

Paired t test	
P value	0.8014
P value summary	ns
Significantly different (P < 0.05)?	No
One- or two-tailed P value?	Two-tailed
t, df	t=0.2583, df=10
Number of pairs	11

Descriptive statistics – combined ACSF

Paired t test Descriptive statistics	Pre-Puff	Post-Puff	Post-Puff - Pre-Puff
Number of values	11	11	11
Minimum	1.333	0.000	-4.000
25% Percentile	1.667	1.000	-1.667
Median	4.000	4.000	-0.6667
75% Percentile	5.667	8.000	2.333
Maximum	14.00	16.00	8.333
Mean	4.909	5.182	0.2727
Std. Deviation	3.633	5.344	3.502
Std. Error of Mean	1.096	1.611	1.056
Lower 95% CI	2.468	1.591	-2.080
Upper 95% CI	7.350	8.772	2.625

Paired t-test and descriptive statistics on whole cell patch puff data of combined ACSF cells displayed in Figure 16 $B_{1,4}$

Paired t-test – LII vehicle

Paired t test	
P value	0.6318
P value summary	ns
Significantly different (P < 0.05)?	No
One- or two-tailed P value?	Two-tailed
t, df	t=0.5047, df=6
Number of pairs	7

Descriptive statistics – LII vehicle

Paired t test Descriptive statistics	Pre-Puff	Post-Puff	Post-Puff - Pre-Puff
Number of values	7	7	7
Minimum	2.333	0.000	-6.000
25% Percentile	5.667	3.000	-1.333
Median	6.667	7.000	0.000
75% Percentile	12.00	12.00	0.6667
Maximum	14.67	31.00	16.33
Mean	8.381	9.714	1.333
Std. Deviation	4.356	10.23	6.989
Std. Error of Mean	1.647	3.865	2.642
Lower 95% CI	4.352	0.2568	-5.131
Upper 95% CI	12.41	19.17	7.797

Paired t-test and descriptive statistics on whole cell patch puff data of LII vehicle cells displayed in Figure 16 $C_{2,4}$

Paired t-test – LIII vehicle

Paired t test	
P value	0.0301
P value summary	*
Significantly different (P < 0.05)?	Yes
One- or two-tailed P value?	Two-tailed
t, df	t=3.893, df=3
Number of pairs	4

Descriptive statistics – LIII vehicle

Paired t test Descriptive statistics	Pre-Puff	Post-Puff	Post-Puff - Pre-Puff
Number of values	4	4	4
Minimum	1.333	0.000	-6.333
25% Percentile	2.500	0.000	-5.833
Median	6.167	1.000	-4.167
75% Percentile	7.833	3.500	-2.000
Maximum	8.333	4.000	-1.333
Mean	5.500	1.500	-4.000
Std. Deviation	2.963	1.915	2.055
Std. Error of Mean	1.481	0.9574	1.027
Lower 95% CI	0.7856	-1.547	-7.270
Upper 95% CI	10.21	4.547	-0.7303

Paired t-test and descriptive statistics on whole cell patch puff data of LIII vehicle cells displayed in Figure 16 $C_{3,4}$

Paired t-test – combined vehicle

Paired t test	
P value	0.7505
P value summary	ns
Significantly different (P < 0.05)?	No
One- or two-tailed P value?	Two-tailed
t, df	t=0.3269, df=10
Number of pairs	11

Descriptive statistics – combined vehicle

Paired t test Descriptive statistics	Pre-Puff	Post-Puff	Post-Puff - Pre-Puff
Number of values	11	11	11
Minimum	1.333	0.000	-6.333
25% Percentile	5.667	0.000	-4.333
Median	6.333	4.000	-1.333
75% Percentile	11.33	10.00	0.3333
Maximum	14.67	31.00	16.33
Mean	7.333	6.727	-0.6061
Std. Deviation	4.017	9.001	6.150
Std. Error of Mean	1.211	2.714	1.854
Lower 95% CI	4.635	0.6803	-4.737
Upper 95% CI	10.03	12.77	3.525

Paired t-test and descriptive statistics on whole cell patch puff data of combined vehicle cells displayed in Figure 16 $C_{1,4}$

Paired t-test – LII 100 µM dopamine

Paired t test	
P value	0.6363
P value summary	ns
Significantly different (P < 0.05)?	No
One- or two-tailed P value?	Two-tailed
t, df	t=0.5110, df=4
Number of pairs	5

Descriptive statistics – LII 100 µM dopamine

Paired t test Descriptive statistics	Pre-Puff	Post-Puff	Post-Puff - Pre-Puff
Number of values	5	5	5
Minimum	1.267	0.000	-5.667
25% Percentile	1.800	0.000	-5.333
Median	5.000	2.000	-2.333
75% Percentile	11.83	12.00	3.367
Maximum	16.67	13.00	8.000
Mean	6.453	5.200	-1.253
Std. Deviation	6.136	6.301	5.484
Std. Error of Mean	2.744	2.818	2.453
Lower 95% CI	-1.165	-2.623	-8.063
Upper 95% CI	14.07	13.02	5.556

Paired t-test and descriptive statistics on whole cell patch puff data of LII 100 µM dopamine treated cells displayed in Figure 16 $D_{2,4}$

Paired t-test – LIII 100 µM dopamine

Paired t test	
P value	0.1918
P value summary	ns
Significantly different (P < 0.05)?	No
One- or two-tailed P value?	Two-tailed
t, df	t=1.569, df=4
Number of pairs	5

Descriptive statistics – LIII 100 µM dopamine

Paired t test Descriptive statistics	Pre-Puff	Post-Puff	Post-Puff - Pre-Puff
Number of values	5	5	5
Minimum	2.667	0.000	-35.67
25% Percentile	3.833	0.000	-22.67
Median	5.333	0.000	-3.333
75% Percentile	22.67	3.500	-1.333
Maximum	35.67	5.000	0.000
Mean	11.67	1.400	-10.27
Std. Deviation	13.65	2.191	14.64
Std. Error of Mean	6.106	0.9798	6.545
Lower 95% CI	-5.285	-1.320	-28.44
Upper 95% CI	28.62	4.120	7.905

Paired t-test and descriptive statistics on whole cell patch puff data of LIII 100 µM dopamine treated cells displayed in Figure 16 $D_{3,4}$

Paired t-test – combined 100 µM dopamine

Paired t test	
P value	0.1462
P value summary	ns
Significantly different (P < 0.05)?	No
One- or two-tailed P value?	Two-tailed
t, df	t=1.591, df=9
Number of pairs	10

Descriptive statistics – combined 100 µM dopamine

Paired t test Descriptive statistics	Pre-Puff	Post-Puff	Post-Puff - Pre-Puff
Number of values	10	10	10
Minimum	1.267	0.000	-35.67
25% Percentile	2.583	0.000	-6.667
Median	5.167	1.000	-3.000
75% Percentile	11.42	6.500	-0.9500
Maximum	35.67	13.00	8.000
Mean	9.060	3.300	-5.760
Std. Deviation	10.35	4.877	11.45
Std. Error of Mean	3.273	1.542	3.621
Lower 95% CI	1.656	-0.1891	-13.95
Upper 95% CI	16.46	6.789	2.432

Paired t-test and descriptive statistics on whole cell patch puff data of combined 100 µM dopamine treated cells displayed in Figure 16 $D_{1,4}$

Appendix D

Two-way ANOVA

ANOVA table	SS	DF	MS	F (DFn, DFd)	P value
Time x Group	12.80	1	12.80	F (1, 20) = 11.21	P=0.0032
Time	12.80	1	12.80	F (1, 20) = 11.21	P=0.0032
Group	16.15	1	16.15	F (1, 20) = 8.274	P=0.0093
Subject	39.03	20	1.952	F (20, 20) = 1.709	P=0.1196
Residual	22.83	20	1.142		

Bonferroni's multiple comparisons test

Bonferroni's multiple	Predicted (LS) mean diff.	95.00% CI of diff.	Significant?	Summary	Adjusted P Value
Dopamine - Control					
Baseline	-0.1333	-1.373 to 1.107	No	ns	>0.9999
Peak	-2.300	-3.540 to -1.060	Yes	***	0.0002

Two-way ANOVA and Bonferroni's multiple comparisons test on spike data displayed in Figure 17 B_1 comparing 100 µM dopamine with time-match ACSF controls.

Two-way ANOVA

ANOVA table	SS	DF	MS	F (DFn, DFd)	P value
Time x Group	71.40	1	71.40	F (1, 20) = 14.65	P=0.0011
Time	89.13	1	89.13	F (1, 20) = 18.28	P=0.0004
Group	165.2	1	165.2	F (1, 20) = 3.998	P=0.0593
Subject	826.5	20	41.33	F (20, 20) = 8.476	P<0.0001
Residual	97.51	20	4.875		

Bonferroni's multiple comparisons test

Bonferroni's multiple	Predicted (LS) mean diff.	95.00% CI of diff.	Significant?	Summary	Adjusted P Value
Dopamine - Control					
BL	-1.333	-6.126 to 3.459	No	ns	>0.9999
Peak	-6.450	-11.24 to -1.657	Yes	**	0.0064

Two-way ANOVA and Bonferroni's multiple comparisons test on membrane potential data displayed in Figure 17 B_1 comparing 100 µM dopamine with time-match ACSF controls.

Two-way ANOVA

ANOVA table	SS	DF	MS	F (DFn, DFd)	P value
Time x Group	11.25	1	11.25	F (1, 8) = 15.00	P=0.0047
Time	11.25	1	11.25	F (1, 8) = 15.00	P=0.0047
Group	18.05	1	18.05	F (1, 8) = 12.89	P=0.0071
Subject	11.20	8	1.400	F (8, 8) = 1.867	P=0.1979
Residual	6.000	8	0.7500		

Bonferroni's multiple comparisons test

Bonferroni's multiple	Mean Diff.	95.00% CI of diff.	Significant?	Summary	Adjusted P Value
Dopamine - Control					
Baseline	-0.4000	-2.022 to 1.222	No	ns	>0.9999
Peak	-3.400	-5.022 to -1.778	Yes	***	0.0002

Two-way ANOVA and Bonferroni's multiple comparisons test on spike data displayed in Figure 17 C_3 comparing LII 100 µM dopamine with time-match ACSF controls.

Two-way ANOVA

ANOVA table	SS	DF	MS	F (DFn, DFd)	P value
Time x Group	72.20	1	72.20	F (1, 8) = 22.56	P=0.0014
Time	72.20	1	72.20	F (1, 8) = 22.56	P=0.0014
Group	192.2	1	192.2	F (1, 8) = 8.736	P=0.0183
Subject	176.0	8	22.00	F (8, 8) = 6.875	P=0.0066
Residual	25.60	8	3.200		

Bonferroni's multiple comparisons test

Bonferroni's multiple	Mean Diff.	95.00% CI of diff.	Significant?	Summary	Adjusted P Value
Dopamine - Control					
BL	-2.400	-7.952 to 3.152	No	ns	0.6018
Peak	-10.00	-15.55 to -4.448	Yes	***	0.0008

Two-way ANOVA and Bonferroni's multiple comparisons test on membrane potential data displayed in Figure 17 C_3 comparing 100 µM dopamine with time-match ACSF controls.

Two-way ANOVA

ANOVA table	SS	DF	MS	F (DFn, DFd)	P value
Time x Group	1590	3	530.0	F (3, 21) = 14.06	P<0.0001
Time	2209	3	736.3	F (3, 21) = 19.53	P<0.0001
Group	1085	1	1085	F (1, 7) = 7.349	P=0.0302
Subject	1033	7	147.6	F (7, 21) = 3.916	P=0.0070
Residual	791.5	21	37.69		

Bonferroni's multiple comparisons test

Bonferroni's multiple	Predicted (LS) mean diff.	95.00% CI of diff.	Significant?	Summary	Adjusted P Value
Dopamine - Control					
Baseline Peak	2.250	-12.21 to 16.71	No	ns	>0.9999
Baseline Steady	2.388	-12.07 to 16.84	No	ns	>0.9999
Treatment Peak	-25.11	-39.57 to -10.66	Yes	***	0.0003
Treatment Steady	-23.71	-38.17 to -9.257	Yes	***	0.0006

Two-way ANOVA and Bonferroni's multiple comparisons test on input resistance (R_{in}) data displayed in Figure 17 C_5 comparing LII 100 µM dopamine with time-match ACSF controls.

Two-way ANOVA

ANOVA table	SS	DF	MS	F (DFn, DFd)	P value
Time x Group	0.0002803	1	0.0002803	F (1, 7) = 0.4022	P=0.5461
Time	6.739e-006	1	6.739e-006	F (1, 7) = 0.009670	P=0.9244
Group	0.01620	1	0.01620	F (1, 7) = 0.7806	P=0.4063
Subject	0.1453	7	0.02075	F (7, 7) = 29.78	P=0.0001
Residual	0.004878	7	0.0006969		

Bonferroni's multiple comparisons test

Bonferroni's multiple	Predicted (LS) mean diff.	95.00% CI of diff.	Significant?	Summary	Adjusted P Value
Dopamine - Control					
Baseline	-0.05243	-0.2268 to 0.1219	No	ns	0.9259
Peak	-0.06831	-0.2426 to 0.1060	No	ns	0.6843

Two-way ANOVA and Bonferroni's multiple comparisons test on ratio data displayed in Figure 17 C_5 comparing LII 100 µM dopamine with time-match ACSF controls.

Two-way ANOVA

ANOVA table	SS	DF	MS	F (DFn, DFd)	P value
Time x Group	3.344	1	3.344	F (1, 10) = 10.74	P=0.0083
Time	5.344	1	5.344	F (1, 10) = 17.16	P=0.0020
Group	9.858	1	9.858	F (1, 10) = 9.300	P=0.0123
Subject	10.60	10	1.060	F (10, 10) = 3.404	P=0.0332
Residual	3.114	10	0.3114		

Bonferroni's multiple comparisons test

Bonferroni's multiple	Predicted (LS) mean diff.	95.00% CI of diff.	Significant?	Summary	Adjusted P Value
Dopamine - Control					
Baseline	-0.5429	-1.718 to 0.6320	No	ns	0.5523
Peak	-2.057	-3.232 to -0.8822	Yes	***	0.0008

Two-way ANOVA and Bonferroni's multiple comparisons test on spike data displayed in Figure 17 D_3 comparing LIII 100 µM dopamine with time-match ACSF controls.

Two-way ANOVA

ANOVA table	SS	DF	MS	F (DFn, DFd)	P value
Time x Group	9.858	1	9.858	F (1, 10) = 1.321	P=0.2771
Time	16.86	1	16.86	F (1, 10) = 2.260	P=0.1637
Group	10.30	1	10.30	F (1, 10) = 0.1648	P=0.6933
Subject	624.8	10	62.48	F (10, 10) = 8.376	P=0.0012
Residual	74.60	10	7.460		

Bonferroni's multiple comparisons test

Bonferroni's multiple	Predicted (LS) mean diff.	95.00% CI of diff.	Significant?	Summary	Adjusted P Value
Dopamine - Control					
BL	-0.02857	-8.419 to 8.362	No	ns	>0.9999
Peak	-2.629	-11.02 to 5.762	No	ns	0.9133

Two-way ANOVA and Bonferroni's multiple comparisons test on membrane potential data displayed in Figure 17 D_3 comparing 100 µM dopamine with time-match ACSF controls.

Two-way ANOVA

ANOVA table	SS	DF	MS	F (DFn, DFd)	P value
Time x Group	477.8	3	159.3	F (3, 30) = 2.168	P=0.1125
Time	30.76	3	10.25	F (3, 30) = 0.1396	P=0.9355
Group	153.2	1	153.2	F (1, 10) = 0.7996	P=0.3922
Subject	1916	10	191.6	F (10, 30) = 2.608	P=0.0206
Residual	2204	30	73.47		

Bonferroni's multiple comparisons test

Bonferroni's multiple	Predicted (LS) mean diff.	95.00% CI of diff.	Significant?	Summary	Adjusted P Value
Dopamine - Control					
Baseline Peak	3.179	-12.37 to 18.72	No	ns	>0.9999
Baseline Steady	2.320	-13.22 to 17.86	No	ns	>0.9999
Treatment Peak	-9.307	-24.85 to 6.238	No	ns	0.5009
Treatment Steady	-10.69	-26.23 to 4.856	No	ns	0.3186

Two-way ANOVA and Bonferroni's multiple comparisons test on input resistance (R_{in}) data displayed in Figure 17 D_5 comparing LIII 100 µM dopamine with time-match ACSF controls.

Two-way ANOVA

ANOVA table	SS	DF	MS	F (DFn, DFd)	P value
Time x Group	5.830e-005	1	5.830e-005	F (1, 10) = 0.1574	P=0.6999
Time	5.535e-005	1	5.535e-005	F (1, 10) = 0.1494	P=0.7072
Group	0.007236	1	0.007236	F (1, 10) = 0.9133	P=0.3618
Subject	0.07923	10	0.007923	F (10, 10) = 21.39	P<0.0001
Residual	0.003704	10	0.0003704		

Bonferroni's multiple comparisons test

Bonferroni's multiple	Predicted (LS) mean diff.	95.00% CI of diff.	Significant?	Summary	Adjusted P Value
Dopamine - Control					
Baseline	0.03206	-0.05931 to 0.1234	No	ns	0.8105
Peak	0.03838	-0.05298 to 0.1297	No	ns	0.6417

Two-way ANOVA and Bonferroni's multiple comparisons test on ratio data displayed in Figure 17 D_5 comparing LIII 100 µM dopamine with time-match ACSF controls.